FISEVIER

Contents lists available at ScienceDirect

## Results in Engineering

journal homepage: www.sciencedirect.com/journal/results-in-engineering



## Research paper

# Shear yield and shear rupture strength of welded brace members under cyclic loading

Shervin Maleki <sup>a</sup>, Kamyab Rezaee <sup>a</sup>, Asal Pournaghshband <sup>b,\*</sup>

- a Department of Civil Engineering, Sharif University of Technology, Azadi Ave., Tehran, Iran
- <sup>b</sup> School of Physics, Engineering and Computer Science, University of Hertfordshire, UK

#### ARTICLE INFO

Keywords: Shear yielding Shear rupture Channel section Base metal strength Steel bracing Gusset plate

#### ABSTRACT

The shear yield (SY) and shear rupture (SR) are two critical failure modes in steel bracing members with welded gusset plate connections. These failures occur near the longitudinal welds in the member and ultimately cause separation of the brace member from the gusset plate. The SY appears as excessive displacement in the member connection region which ultimately leads to SR failure and separation. Existing research on these phenomena in welded braces is limited, particularly under compressive and cyclic loading conditions. Current studies focus mainly on monotonic tensile loading. This is despite the fact that braces are commonly subjected to reversible loads such as those from wind and seismic events. Compressive loads induce local buckling, and cyclic loading causes low-cycle fatigue, both of which significantly influence failure patterns. This study investigates the SY and SR behaviours of welded single and double-channel members under tensile, compressive, and cyclic loads. Nonlinear finite element (FE) models with ductile fracture prediction capabilities were developed and validated against experimental results. Eight specimens with varying channel sizes, gusset dimensions, weld lengths and throat thicknesses were analysed. The load-displacement results were plotted and compared, and the applicability of AISC design strength equations were evaluated. Results showed that AISC equations provide conservative estimates for monotonic loading. However, under cyclic loading, the equations slightly overestimate the shear rupture strength in some cases but remain generally safe if excessive deformation is acceptable. This research provides a detailed numerical investigations of SY and SR under compressive and cyclic loads. It highlights the effects of low-cycle fatigue and local buckling on shear capacity and failure patterns. These findings address gaps in design standards and improve the safety and reliability of welded brace connections in structures exposed to reversible loading conditions.

## 1. Introduction

Steel braced frames with gusset plate connections are economical and easily adaptable to various functional and architectural needs, making them a common choice for lateral force-resisting systems. However, instances of fatigue failure in gusset plates have been observed during major earthquakes, including the 2011 Christchurch Earthquake in New Zealand [1,2], highlighting the need for improved design considerations. In special concentrically braced frame (SCBF) systems, which are designed to dissipate earthquake energy through brace yielding and buckling deformation in the vicinity of mid brace length, various undesirable failure modes have been observed during the past seismic events. These include: fracture of the welds at the gusset plate interface, tearing or buckling of the gusset plate, net section failure of

the brace cross-section, shear failure of the brace or gusset plate, and premature failure of the brace section. Such failures can compromise the system's performance and highlight critical areas requiring attention in seismic design.

The reliability of design codes, such as the AISC [3,4], is paramount for ensuring the safety and resilience of structures subjected to extreme loading conditions, including earthquakes and wind forces. These codes serve as the foundation for structural design. However, their provisions for shear yield (SY) and shear rupture (SR), the key failure modes in brace to gusset connections, need further verification due to complex nature of these forces in welded brace members. Accurate evaluation of these provisions is crucial to confirm that they provide sufficient safety margins and reflect the actual performance of braces under realistic cyclic loading conditions, safeguarding structural integrity and public

E-mail address: a.pournaghshband@herts.ac.uk (A. Pournaghshband).

<sup>\*</sup> Corresponding author.

safety. In this context, Ghaderi-Garekani and Maleki [5] examined SY and SR in welded channel and angle brace members connected to gusset plates under tensile loading. Using finite element (FE) models, they assessed AISC design provisions and proposed modifications to improve prediction accuracy. Fortney et al. [6] provided guidance on shear rupture, ductility, and element capacity in welded connections, focusing on misunderstood and misapplied limit state checks. Their work reviewed the AISC Specification and highlighted areas for improving design consistency but did not conduct an explicit assessment of the code's adequacy.

Most research studies concentrate on the capacity of the brace member and not its connections. Zhang et al. [7], investigated the effectiveness of the Chinese design code GB 50,011-2010 through experimental investigations by focusing on the cyclic behaviour of H-shaped steel bracing members with bolted gusset plate connections. Their study also proposed simplified design recommendations to enhance seismic performance. Building on this work, Xie and Zhang [8] conducted numerical analyses on similar connections, focusing on hysteretic performance, low-cycle fatigue life, and internal force mechanisms. Their study evaluated the applicability of ANSI/AISC 341–16 and GB 50,011-2010 design codes, offering insights to improve code accuracy and reliability. Likewise, the seismic provisions for special concentrically braced frames (SCBF) in AISC 341-22 were critically evaluated by Shen et al. [9], focusing on the inelastic cyclic deformation capacity of braces. Drawing on over 40 years of experimental data, the study identified potential deficiencies in the provisions related to ensuring sufficient ductility and preventing premature failures during seismic events.

Past research devoted to the study of SR and SY limit states in members of welded brace connections is scarce. The published research is mainly devoted to bolted connections [10–12]. In addition, the limited studies available for welded connections considered only tensile loading. Here, only those with welded connections as related to the context of this paper are briefly reviewed. The SY strength of gusset plates in lap splice welded joints was studied by Nguyen [13]. This study proved that the AISC shear yield equation (Eq. (2) below) is very conservative and a length increase in the shear line was suggested to match the experimental data. Also, Topkaya [14] investigated the block shear capacity of gusset plates in welded lap joints. He also found that the AISC block shear equation is conservative to use for gusset plates.

The first author in a series of papers [15–17] has investigated the SY, SR and BS strengths of welded members and gusset plates under tensile loading including eccentric loads. More recently, Ghaderi-Garekani and Maleki [5] studied the SY and SR strength of channel and angle brace members under monotonic tensile loading. This paper intends to study numerically the shear rupture (SR) and shear yield (SY) strengths of single and double-channel braces in the vicinity of longitudinal welds and find the associated failure patterns in the member under tensile, compressive and cyclic loading. The originality of this research lies in addressing unresolved design questions on the shear yielding and rupture behavior of welded single- and double-channel brace members under compressive and cyclic loading, and in systematically evaluating the adequacy of AISC J4 provisions beyond their conventional monotonic-tension basis. The previous research [5] had only considered tensile loading. However, compressive loading can cause local buckling in the channel web and flanges. This in return can affect the shear failure capacity and failure pattern in the channel and has not been investigated before. The application of cyclic load also investigates the possibility of low cycle fatigue failure as it happens under earthquake loading. It should be noted that while overall brace or gusset buckling is not considered in this study, the FE analyses capture local buckling of channel flanges and webs. This local instability is shown in later sections to directly affect the shear rupture capacity. Therefore, compressive loading remains an essential novelty of this work, since the interaction between local buckling and shear limit states has not been addressed in prior research.

In recent years, the state of research on gusset connections has expanded with a focus on cyclic loading, fatigue and seismic relevance. A comprehensive 2023 review by Song et al. [18] synthesizes current design approaches, failure modes (e.g., block-shear, plate buckling, weld-metal interaction), and highlights the urgent need for cyclic and fatigue-oriented investigations in gusset plate behavior. Concurrently, Zhang et al. [19] provide experimental data on low-cycle fatigue performance of concentrically braced H-shaped members with bolted gusset connections, showing how bolt slippage and connection clearances significantly influence strength, energy dissipation, and deformability.

In this study, the AISC J4 provisions for SY and SR are systematically evaluated not only under monotonic tension but also under compression and cyclic loading. The aim is to quantify the conservatism of the code predictions, to identify conditions where they may slightly overestimate or underestimate strengths, and to provide insight into whether these provisions remain safe and reliable across a broader loading spectrum than currently validated. Hence, this work positions itself as both a critique and a confirmation: the equations are shown to be conservative in most cases, but refinements may be warranted in the presence of cyclic degradation and local buckling.

From a practical perspective, gusset plate and welded channel connections have been observed to suffer premature damage in past earthquakes, often associated with shear rupture or local instability at the weld region. Recent experimental studies have also indicated that the AISC J4 shear rupture provisions, while conservative for monotonic tension, may be unconservative under certain compression and cyclic loading regimes. These concerns raise important design questions for practicing engineers, especially in seismic regions where brace—gusset connections govern system performance. To address these issues, the present study not only develops a detailed finite element framework but also validates it against experimental data, ensuring that the numerical predictions are anchored in physical behavior. This dual approach provides practicing engineers and code developers with both critical evaluation of the current AISC provisions and reliable data for refining design guidance.

Despite extensive research on bolted and gusseted brace connections, comparatively little attention has been given to welded channel braces, particularly under combined compressive and cyclic loading. Existing studies focus mainly on overall buckling or bolted gusset behavior, leaving the shear rupture and shear yield mechanisms of welded channel—gusset interfaces largely unexamined. This gap is significant for seismic design, where welded connections are increasingly adopted for ease of fabrication and improved stiffness. The present study addresses this gap through a detailed finite element investigation of welded single-and double-channel braces, emphasizing shear rupture (SR) and shear yield (SY) behavior under monotonic and cyclic loading.

## 2. Research approach and objectives

Steel rolled channel sections (called C-sections in the USA or UNP in Europe) are used as bracing members in many structures to resist lateral forces such as wind and earthquake. In welded single-channel gusset plate connections, as illustrated in Fig. 1(a), commonly the channel is welded at its flanges. This will increase the out of plane radius of gyration and increases the buckling capacity in that direction. This is further enhanced by using two channel sections welded at flanges in a so-called toe-to-toe arrangement (Fig. 1(b)). In contrast, in bolted brace connections the channel web is attached to the gusset plate to facilitate bolting in a back-to-back arrangement.

According to the current American steel design standard AISC [3], in welded joints like that shown in Fig. 1, the connection strength may be governed by the weld metal strength or the base metal (BM) strength. The BM strength should consider the connecting element (i.e., the gusset plate) and the member (i.e., the channel section) strength as the weld is attached to both. The member strength at the connection is addressed in AISC J4 in which, the strength is determined in accordance with the

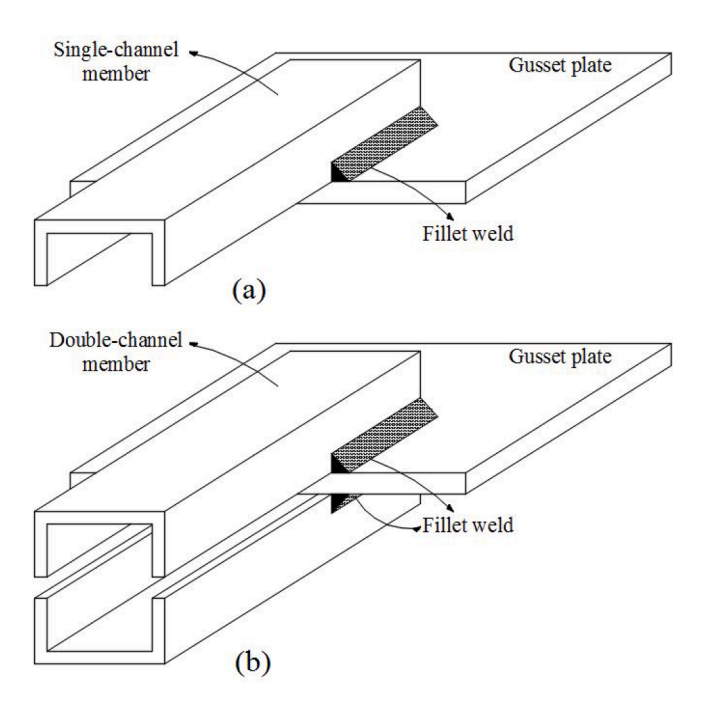


**Fig. 1.** Schematic view of welded (a) single and (b) double channel member to gusset plate.

limit states of tensile rupture (TR), shear yielding (SY), shear rupture (SR), and block shear (BS). In welded end connections with longitudinal fillet weld lines, SY and SR are the probable failure modes when a short weld length is used while the TR governs when a long fillet weld is employed. Unlike the SR limit state, SY only represents yielding and is not accompanied by separation in the base metal and hence in reality always occurs prior to the SR failure. Therefore, it seems that the limit state of SY should not be considered as an independent ultimate limit state in the shear strength check of welded brace members and it is only critical when yield displacement in the connection region is a major design concern. Note that, under compressive loading the shear rupture area remains the same but local buckling can alter the strength available. Also, under compressive loading, the tensile separation is unlikely to occur. In addition, under cyclic loading low cycle fatigue can also reduce the shear capacity. These cases are not widely considered previously and are discussed in this paper for the first time. This study is a detailed analysis of welded single- and double-channel braces under compressive and cyclic loading with ductile damage based rupture tracking.

In this regard, first, nonlinear finite element (FE) models with ductile damage prediction capability were developed and validated against available test results (one test by the first author) on welded gusset plate connections. Note that, the addition of ductile damage to FE models was to ascertain that SR failure pattern is the governing mode of failure. Otherwise, the ultimate strength of the connection is not significantly affected by damage modeling. Then, nonlinear FE models of eight specimens with different channel sizes and weld lengths and thicknesses and gusset sizes were analysed. The models were subjected to tensile, compressive and cyclic loads. The load-displacement results were plotted and compared. The suggested AISC equations for SY and SR limit states were also evaluated for each case. Through FE nonlinear geometry and material modelling with ductile damage consideration the actual failure patterns were obtained that include the effects of the load transfer path, the low cycle fatigue, local buckling and stress concentration phenomena.

#### 3. SY and SR limit states in the AISC specification

In a welded channel to gusset connections as shown in Fig. 2, the connection capacity is governed by the strength of either the base metal (BM) or the deposited fillet weld metal. The base metal failure is described in section J4 of the American Specification for Structural Steel Buildings, AISC [3]. The figure depicts a single-channel brace member under tensile axial loading welded to a gusset plate by means of two longitudinal fillet weld lines. The stress distribution in the channel member is changed from uniform distribution to a non-uniform distribution at the junction with the gusset plate due to shear lag and stress concentration.

Considering the load transfer path shown in Fig. 2, it is noted that Section 1 is where gross tensile yielding (TY) of the section might occur. Section 2 is the effective tension area, in which tensile rupture (TR) can occur and includes the effect of shear lag and load eccentricity. On the other hand, Section 3 is the gross area subjected to shear and is the subject of this paper's investigation. It should be noted that, the gross and the net shear areas (Section 3) are equal to each other in welded joints. Considering the connection geometry shown in Fig. 2, L is the connection length and  $t_f$  is the channel flange thickness in the vicinity of the weld. Hence, to calculate the design strength in shear according to AISC, the gross ( $A_{gv}$ ) and net shear area ( $A_{nv}$ ), shown as cross hatched area, are equal to each other and can be found as follows:

$$A_{gv} = A_{nv} = 2Lt_f \tag{1}$$

Consequently, according to AISC [3], the SY and SR nominal strengths of the channel member can be estimated using the following equations:

$$R_{n1} = 0.6F_{\gamma}A_{g\nu} \tag{2}$$

$$R_{n2}=0.6F_uA_{n\nu} \tag{3}$$

Where  $F_y$  and  $F_u$  are the yield and tensile strengths of the flange steel material, respectively. Moreover, the strength reduction factors  $(\phi)$  of 1.00 and 0.75 are applied respectively to the above nominal strengths to obtain the design strengths for the two limit states, respectively.

Considering the above design strength equations and knowing the shear areas are the same, it is clear that in welded connections the SY nominal strength is always lower than SR. However, the higher strength reduction factor of 1.0 for SY may compensate for this shortcoming and establishes a balance between the SY and SR design strengths. In other words, for steels with an ultimate-to-yield strength ratio greater than 1.33, SY governs, otherwise, SR will be the governing limit state. Given that common mild steels (e.g., A36, S235, and S275) used in bracing members have an ultimate-to-yield strength ratios greater than 1.33, the SY limit state always governs the member design strength in shear. Also, in other commonly used steels (e.g., A992 for shapes and A500 Grade C for HSS members), the ultimate-to-yield strength ratios are very close to 1.3 and the SY and SR limit states provide almost equal design strengths.

## 4. Numerical analysis and FE modelling

In this study, Abaqus finite element software [20] was used for numerical modelling of welded member to gusset connections considering nonlinear material and geometry. The study aims to numerically evaluate the shear yield (SY) and shear rupture (SR) failure modes of welded joints under monotonic and cyclic loading in the brace member. The FE models are composed of three parts: channel member, gusset plate, and longitudinal welds.

#### 4.1. Models geometry

To consider various parameters involved in the shear strength of a member at the welded connection, different channel profiles along with

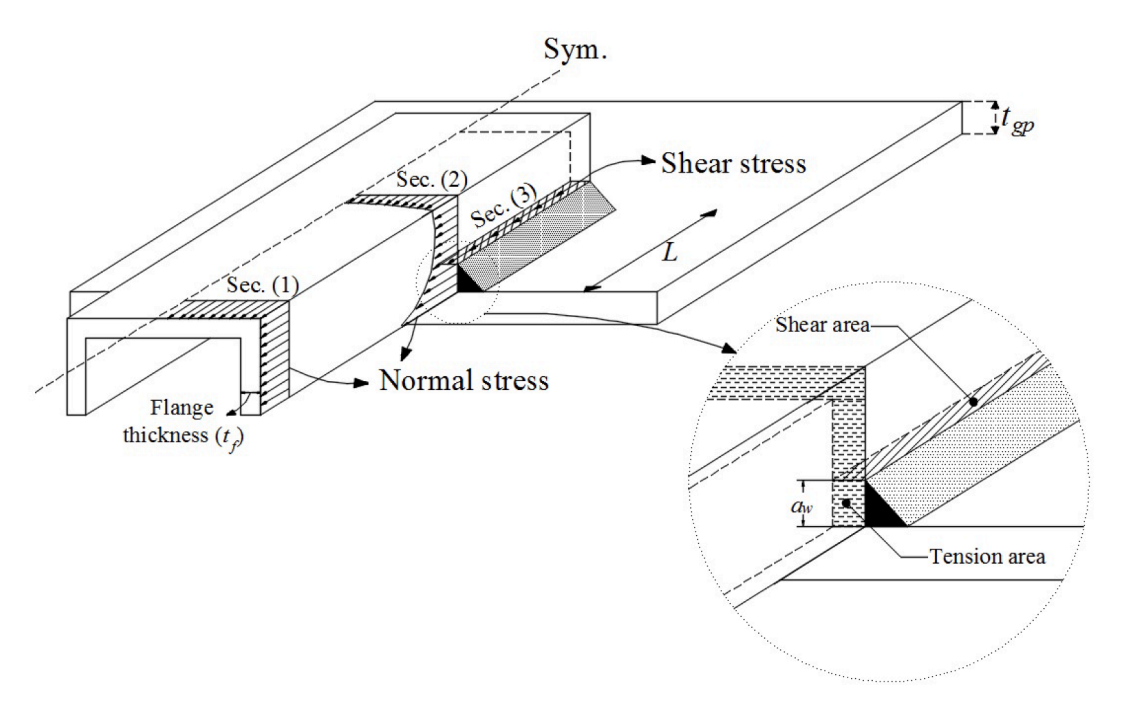


Fig. 2. Load transfer in a typical welded channel to gusset plate connection.

different fillet weld sizes, gusset plate sizes and weld lengths were modelled in the FE software. The geometry of single and double-channel profile models is shown in Fig. 3. Both flanges of a channel are welded to the gusset plate using fillet welds from the outside of the channels.

## 4.2. FE meshing

Among the different meshing types for solid structures, all components of the models were meshed using three-dimensional 8-node solid elements with reduced integration and linear geometric order (C3D8R). C3D8R elements were selected because they have been widely validated for nonlinear steel connection modelling, particularly where large deformations, contact interactions, and ductile damage are involved. Prior studies on gusset plate and brace modelling have shown that C3D8R offers a good balance of computational efficiency and accuracy in predicting shear failure paths. A mesh convergence study was performed to verify that the adopted element size provides mesh-independent results. In earlier studies by the first author on welded gusset plate connections, seed sizes of 4–5 mm in the vicinity of the weld were shown to accurately capture shear yielding and rupture. Following this precedent, several

models were checked in the present study; however, for brevity, only the results for the double-channel specimen shown in Fig. 4 are presented here. The adopted mesh scheme used a 5 mm seed size around the weld and other critical regions, with coarser elements applied in non-critical zones to reduce computational cost (Fig. 4(a)). To further confirm the adopted mesh selection, two additional analyses were conducted on this model: first with a uniform 5 mm mesh across the entire structure (Fig. 4(b)), and second with a uniform 4 mm mesh for the entire structure (Fig. 4(c)). Comparisons among these cases are shown in Fig. 4 parts (d), (e) and (f). Negligible differences in load–displacement curves, ultimate capacity, and rupture mode were observed. Therefore, the adopted mesh strategy (5 mm in critical zones, larger elsewhere) is confirmed to be adequate for accurate and efficient prediction of SY and SR behavior.

## 4.3. Boundary conditions

To save time, symmetry option of the software was used as boundary condition. Also, boundary conditions were chosen to replicate laboratory subassembly test setups. For single channel models, only half of the gusset and channel profile were modelled. For double channels, half of

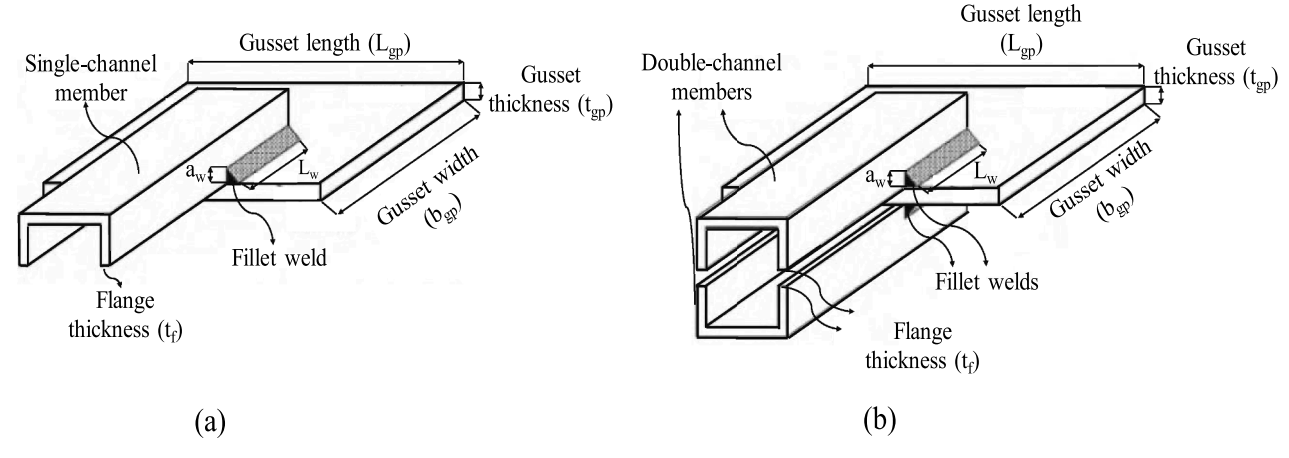


Fig. 3. Structural models investigated with (a) single channel and (b) double channel sections.

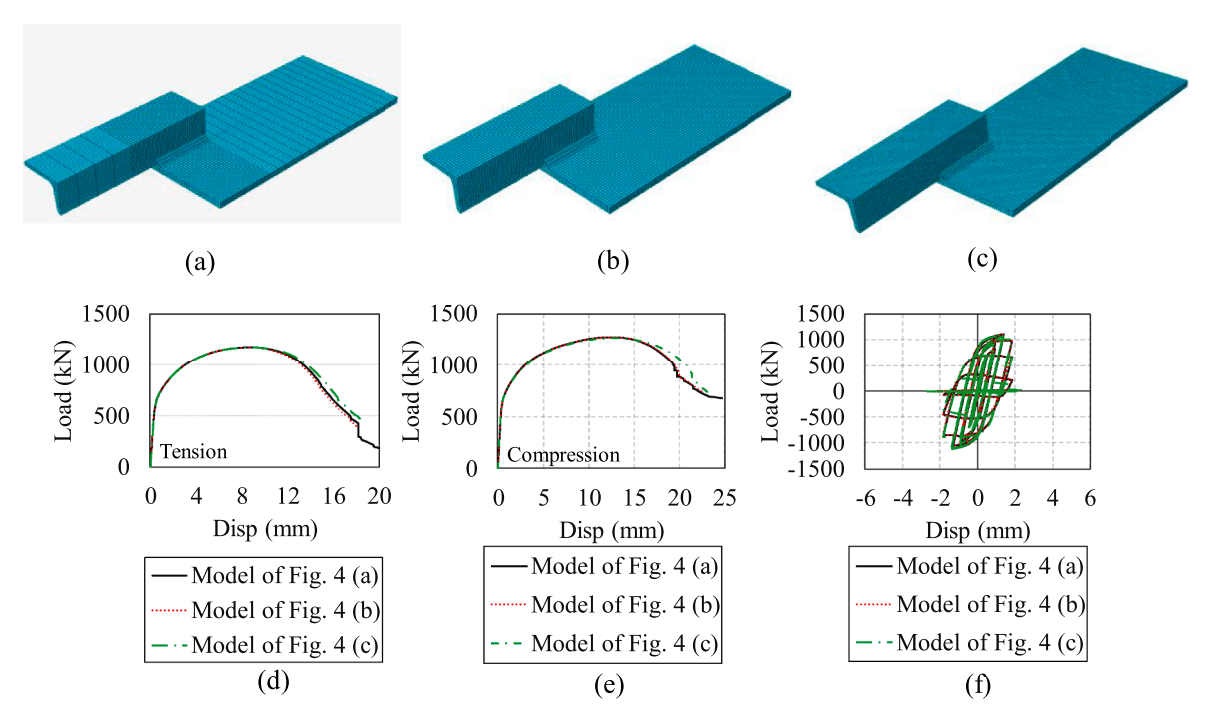


Fig. 4. (a) to (c) Meshed structures using dual symmetry for a typical double channel section. Parts (d) to (e) show the effects of using varying mesh sizes on the load-displacement curves.

the gusset width and thickness and half of the channel profiles were modelled. For single channels, the X symmetry boundary condition was assigned to the edge of channel web and gusset plate as shown in Fig. 5 (a). In case of double channels, both X and Y symmetry boundary conditions were assigned to the appropriate surfaces as shown in Fig. 5(b). In models with single channel, the gusset plate is restricted to translate along the Y axis to prevent buckling of the plate. The end of the channel was fully restrained against both translational and rotational degrees of freedoms. Displacement loading was applied to the end of the gusset along the Z axis.

## 4.4. Constraints and interactions

The adjacent surfaces between the weld to the channel and the weld to the gusset plate were tied together. Surface-based tie constraints were used to model welds because they effectively transfer shear and normal stresses between the channel flange and gusset plate without introducing excessive artificial stiffness. This simplification has been widely applied in previous welded connection studies [21,22], and comparative checks showed that SR predictions were not significantly sensitive to this modelling choice. The constraint makes all displacements and rotations between two adjacent surfaces equal. In order to avoid surface penetration of the components into each other, the interaction between the channel flanges and the gusset plate was modelled as hard contact.

## 4.5. Material behaviour

## 4.5.1. Constitutive relationship of steel

The S235 structural steel, with a modulus of elasticity of 203,806 MPa, Poisson's ratio of 0.3, yield strength of 268 MPa, and ultimate strength of 418 MPa, was utilized in this study. The stress–strain data were extracted directly from the coupon test results of S235 structural steel, as reported by Zhu et al. [23]. This was adopted because the FE

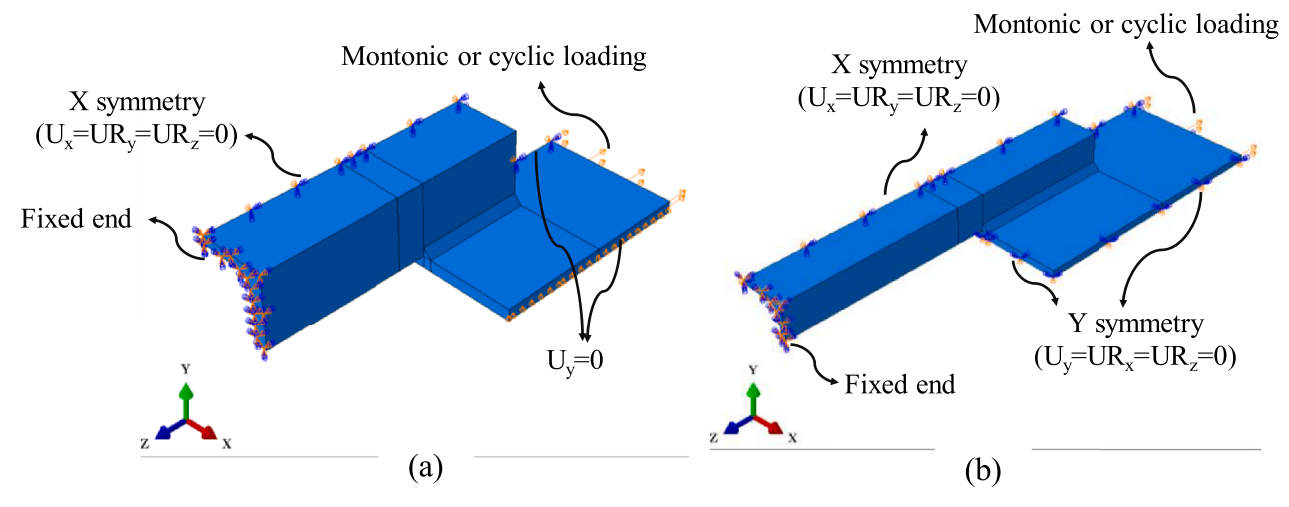


Fig. 5. Boundary conditions for (a) single-channel and (b) double-channel FE models.

model validation was based on the tests conducted by the same authors. In Abaqus software, a plastic isotropic hardening material model with the von Mises flow rule as a yield criterion was implemented to simulate the behaviour of S235 steel in this study. The true stresses and strains were calculated from the engineering stress–strain curve obtained from the coupon test using Eqs. (4) and (5). The calculated true stresses and strains then used in the software.

$$\sigma_{true} = \sigma_{eng}(1 + \varepsilon_{eng}) \tag{4}$$

$$\varepsilon_{true}^{p} = \ln(1 + \varepsilon_{eng}) - \frac{\sigma_{true}}{F} \tag{5}$$

Where,  $\sigma_{eng}$  and  $\varepsilon_{eng}$  represent the engineering stress and strain, respectively, while E denotes the modulus of elasticity. Eqs. (4) and (5) are applicable until the onset of necking, where the strain distribution becomes nonuniform along the specimen gauge length. Subsequently, the "Power Law," was employed to extrapolate the stress–strain curve after the necking phenomenon as follows (Eq. (6)),

$$\sigma = K\varepsilon^m \tag{6}$$

Where k and m are the stiffness coefficient and strain hardening exponent, respectively, obtained by fitting the true stress-strain data points from the yield to the post-necking stage. For the steel under consideration the values of 673.5 and 0.19 are obtained for k and m, respectively. The resulting extended true stress-strain curve according to the coupon test data [23] is shown in Fig. 6.

## 4.5.2. Ductile damage modelling

To assess the rupture path of the modelled connections under monotonic (tension and compression) and cyclic loading, the Damage for Ductile Metals (DDM) option of Abaqus was utilized. Note that, the addition of ductile damage does not affect the actual SR ultimate load carried, which is the main concern of this paper. This continuum damage model can be used in tension, compression and shear loading. It has also been used under cyclic loading with success [8]. The micromechanics models such as Cyclic Void Growth Model (CVGM) has been used to simulate ultra-low cycle fatigue in the middle portion of the braces where plastic hinges develop and crack under repetitive loading. The focus of this study is in the end connection of the braces and such models are not deemed necessary.

In the DDM approach, as the equivalent plastic strain  $(\varepsilon^{pl})$  reaches the failure strain  $(\varepsilon^{pl})$ , the damage is initiated. Additionally, it is hypothesized that the fracture initiation strain is a function of stress triaxiality. Stress triaxiality  $(\eta)$  is the ratio of the hydrostatic stress  $(\sigma_m)$  to the von Mises stress  $(\sigma)$ . These parameters are shown in Eqs. (7) to 9.

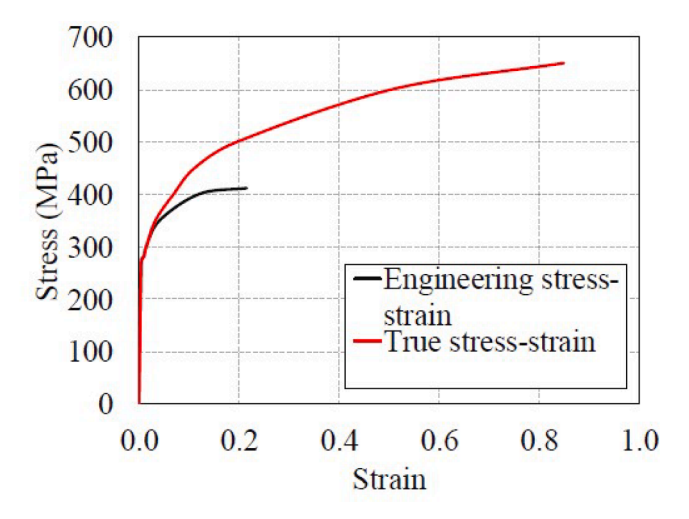


Fig. 6. Stress-strain curve for S235 steel.

$$\eta = \frac{\sigma_m}{\sigma} \tag{7}$$

$$\sigma_{m} = \frac{\sigma_{1} + \sigma_{2} + \sigma_{3}}{3} \tag{8}$$

$$\sigma = \sqrt{\frac{1}{2}[(\sigma_1 - \sigma_2)^2 + (\sigma_2 - \sigma_3)^2 + (\sigma_1 - \sigma_3)^2}$$
 (9)

The failure strain  $(\epsilon_0^{pl})$  is calculated using the Eq. (10). In this paper, a triaxiality-dependent fracture criterion calibrated for industrial aluminium and steel, as described by Lee and Wierzbicki [24], was used (see Eq. (10)).

$$\varepsilon_{0}^{pl} = \begin{cases}
\infty & \eta < -\frac{1}{3} \\
\frac{C_{1}}{1+3\eta} & -\frac{1}{3} < \eta < 0 \\
C_{1} + (C_{2} - C_{1}) \left(\frac{\eta}{\eta_{0}}\right)^{2} & 0 < \eta < \eta_{0} \\
C_{2} \left(\frac{\eta}{\eta_{0}}\right) & \eta > \eta_{0}
\end{cases}$$
(10)

Where,  $C_2$  is ductility of a material and can be obtained from Eq. (11). The parameter  $A_R$  is the reduction in area of a standard tensile test specimen. Additionally, the coefficient  $C_1$  can be determined using Eq. (12). In this formula, m is the strain-hardening exponent introduced in Eq. (6).

$$C_2 = -\ln(1 - A_R) \tag{11}$$

$$C_1 = C_2 \left(\frac{\sqrt{3}}{2}\right)^m \tag{12}$$

Note that these parameters depend on mesh size and type of loading as well. In addition, the actual A<sub>R</sub> is not available. Therefore, for each FE validation model (see Section 4.7) the value of C2 was obtained by trial and error process to match the damage observed in the tests. The value of m = 0.19 for S235 steel. Then, C1 can be obtained from Eq. (12) and  $\varepsilon_0^{\rm pl}$  from Eq. (10). Once damage is initiated, the modulus of elasticity E decreases until the equivalent plastic strain reaches the ultimate failure strain  $\varepsilon_f^{pl}$ , which is the point at which the element is deleted. To capture the post-peak softening response, the progressive damage evolution option in Abaqus, accompanied by a linear softening law, was activated. The stress-strain curve with progressive damage degradation starting at D=0 is shown in Fig. 7. In this figure,  $\sigma_{v0}$  represents the stress at the onset of damage and D represents the overall damage variable, which captures the combined effect of all active damage mechanisms. Additionally, the ultimate failure strain occurs when the overall damage variable is equal to one.

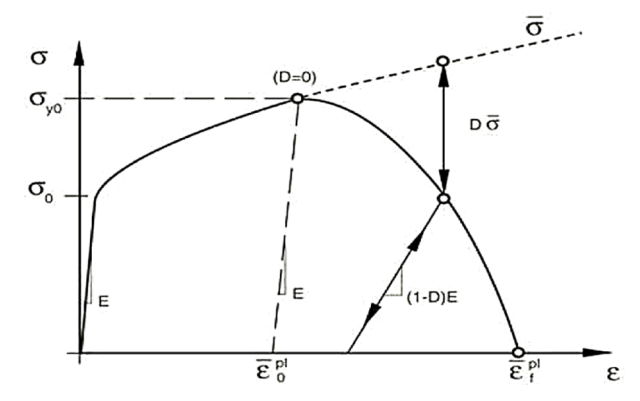


Fig. 7. The stress-strain curve with progressive damage degradation.

#### 4.6. Loading on the structure

## 4.6.1. Monotonic loading

In this study, both monotonic tensile and compressive loads were considered. The loads are applied to the structures using a static-general step defined in Abaqus software. As in the experimental tests, the loads are applied to the structure as displacement controlled, using a ramp function. A large target displacement of 60 mm was used in Abaqus.

## 4.6.2. Cyclic loading

The cyclic displacement loading applied to the end of the gusset plate followed the ATC-24 [25] cyclic loading protocol. The ATC-24 cyclic displacement protocol was selected because it is a widely adopted standard for evaluating low-cycle fatigue and seismic performance of braced frame components, allowing direct comparison of the present results with existing cyclic gusset and brace studies. Accordingly, the yield displacement  $(\Delta_y)$  for each model was first determined using a monotonic tensile loading. The ATC protocol initially calls for six cycles with peak deformation less than the yield displacement followed by three cycles with peak deformation equal to yield displacement. Thereafter, in each subsequent phases, three cycles with peak deformation equal to 3 to 6 times the yield displacement are imposed. The resulting cyclic loading is presented in Fig. 8.

## 4.7. Validation of FE models

To validate the finite element (FE) modelling technique, four instances of welded gusset plate connections were modelled with the aforementioned assumptions. These experiments comprise a welded double-angle to gusset plate connection tested by the first author [17] and three welded angles to gusset plate connections tested by Zhu et al. [23].

## 4.7.1. The experiment by the first author [17]

The objective of this test was to examine the block shear failure mode in welded gusset plates [17]. Therefore, a welded double-angle to gusset plate connection was designed. Given the general similarity of the SR and BS failure modes, this specimen is employed in the present study to validate the finite element (FE) modelling procedure. The dimensions of the gusset plate are 28 cm in width, length, and with a thickness of 0.5 cm. Two angle members are welded to the gusset plate in a manner analogous to the channels depicted in Fig. 3. The angle section is L80  $\times$  80  $\times$  8. The member was fillet-welded to the gusset plate using the Gas Metal Arc Welding (GMAW) process. In accordance with the provisions set forth by the American Welding Society (AWS), the E70 electrode was utilized for the welding process. In this section, S235 steel was employed. A DARTEC universal testing machine was used to test the specimen in tension under a displacement-control monotonic loading

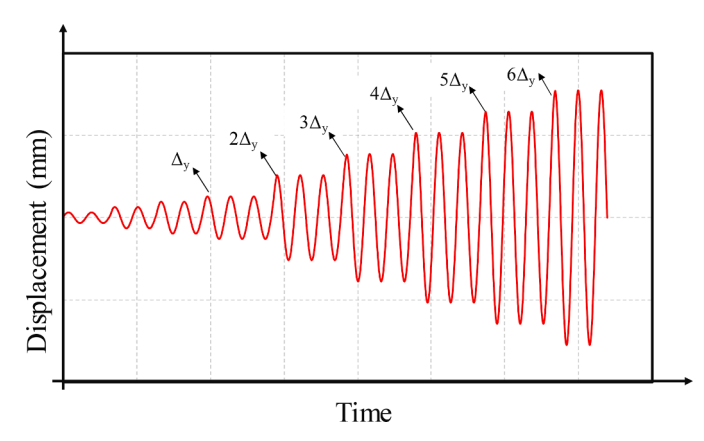


Fig. 8. Applied cyclic displacement loading.

protocol with a rate of 0.05 mm/sec. The test setup is presented in Fig. 9. The results of the tests demonstrated that the block shear mode occurs in the gusset plate. The above structure was modelled in Abaqus, and after the FE analysis, load-displacement curves were obtained. These curves are compared with the experimental results. According to Fig. 10, the FE and experimental results are in good agreement up to the peak load and FE model fails a little earlier. The fractured specimens in both FE and experimental results are shown in Fig. 11. The failure pattern in Fig. 11 shows that the ductile damage model can accurately predict the failure pattern in welded connections.

## 4.7.2. The experiments by Zhu et al. [23]

For the case of welded single angle to gusset plate connection, three specimens from the study of Zhu et al. [23] were modelled for FE analyses. Similar to their study, coupon test data were considered and S235 steel with yield strength of 268 MPa and ultimate strength of 418 MPa was used in the FE modelling. Further details of the specimens of Zhu et al. are shown in Table 1. The load-displacement curves of the FE models and experimental analysis of Zhu et al. are shown in Fig. 12. The figure shows excellent agreement between FE and experimental results. Finally, Fig. 13 shows that the failure patterns are consistent, which confirms the validity of the damage model used in Abaqus.

## 5. Numerical results and discussion

In this study, FE analyses were used to evaluate the SY and SR strength of brace members under tensile, compressive and cyclic loading. In addition, parameters affecting these limit states were varied. These parameters included: weld length  $(l_w)$ , gusset plate thickness  $(t_{gp})$ , weld size  $(a_w)$  and channel size (UNP).

## 5.1. Specimens details for current study

The description of the single-channel and double-channel models considered for FE analyses of this study are presented in Table 2. The models are identified by a name composed of four distinct components: the channel profile size, weld length, gusset thickness, and weld size. For example, the model labelled 2U160–110–25–12 comprises a double channel section of UNP160 connected by longitudinal weld lines measuring 110 mm in length and 12 mm in weld size to a 25 mm thick gusset plate.

## 5.2. Rupture modes

## 5.2.1. Monotonic loading

Under uniform tension, the equivalent plastic strain (PEEQ) contours for a single-channel member (U60–50–8–6) under monotonic tension at three distinct stages (the SY, SR, and final rupture) is illustrated in Fig. 14. All models initially reached their SY strength first, followed by the SR strength and finally ruptured (complete separation). The figures demonstrate that at the point of contact between the channel and the edge of the gusset plate, there is a concentration of plastic strain. From this point, the rupture initiates and subsequently propagates in a direction parallel to the weld. In cases of double-channels, such as 2U160–110–25–12 model, a similar rupture path is observed (see Fig. 15). Furthermore, a similar rupture path occurs in larger models for both single and double-channel members.

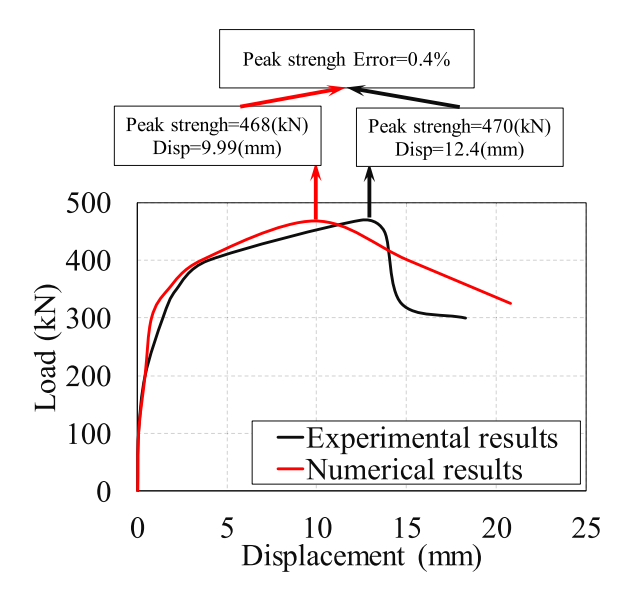
Similar to the cases under uniform tensile loading, a shear rupture occurred in all models under monotonic compression (Figs. 16 and 17). In comparison to the cases under tensile loading, the PEEQ values at the final rupture are much higher under monotonic compression. This indicates that failure under compression is delayed due to cracks closing in compression.

#### 5.2.2. Cyclic loading

The failure path under cyclic loading for single and double-channel



**Fig. 9.** Test setup [17].



 $\textbf{Fig. 10.} \ \ \text{Load-displacement curves of the FE model and test result.}$ 

models is illustrated in Fig. 18 for the U60–50–8–6 and 2U160–110–25–12 models from both sides. In the models with single or double-channel members subjected to cyclic loading, the rupture path exhibits similarities to that observed under monotonic loading. A similar trend was observed for larger models.

To further illustrate the fracture mechanisms, von Mises stress and DUCTCRT damage initiation contours were extracted for the representative models (Fig. 19). These plots show that stress demand is concentrated along the weld line, with local intensification at both weld ends. The DUCTCRT contours confirm that rupture consistently initiates near the gusset-plate end of the weld and subsequently propagates along the weld direction. This observation aligns with the PEEQ concentration patterns discussed earlier and provides a mechanistic basis for the modelled crack paths. In practice, such rupture would likely manifest during post-event inspections as tearing or weld-toe fractures localized at the gusset end of the weld.

## 5.3. Load-displacement curves

The load-displacement curves for single and double-channel members under monotonic loading are presented in Figs. 20 and 21, while Figs. 22 and 23 show similar curves under cyclic loading. In these figures, the vertical axis represents the load capacity, while the horizontal

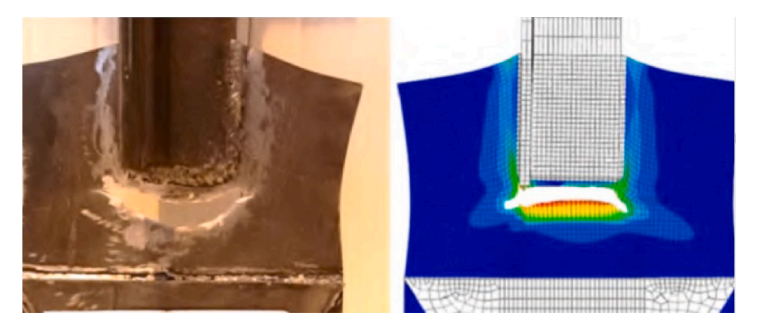


Fig. 11. The experimentally fractured specimen vs numerically fractured specimen.

Table 1 Specimens details and analyses results summary of specimens tested by Zhu et al., [23].

Specimen	Member	Gusset thickness (mm)	Connection length (mm)	Failure mode (test)	Failure mode (FE)	P <sub>u test</sub> (kN)	P <sub>u FE</sub> (kN)	Error %
L1	L 125 75 10	16.0	200	Gusset failure	Gusset failure	786	760	3.31
L2 L3	L 125 75 10 L 125 75 10	16.0 16.0	250 300	Gusset failure Gusset failure	Gusset failure Gusset failure	782 756	777 751	0.64 0.66
LO	L 123 /3 10	10.0	300	Gusset fallule	Gusset fallule	/ 30	/31	0.00

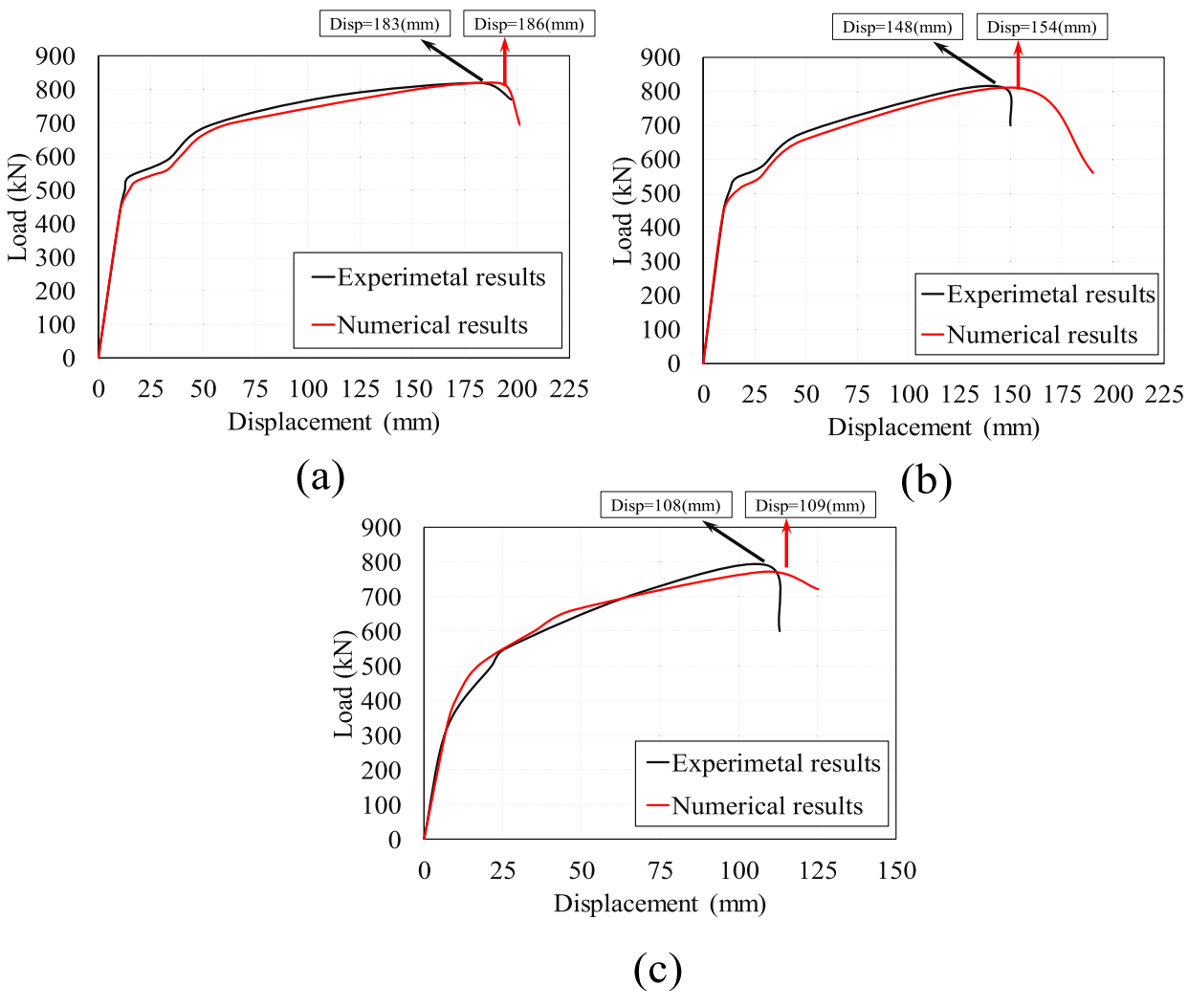


Fig. 12. Comparison of the FE model and experimental results of specimens (a) L1, (b) L2 and (c) L3 tested by Zhu et al., [23].

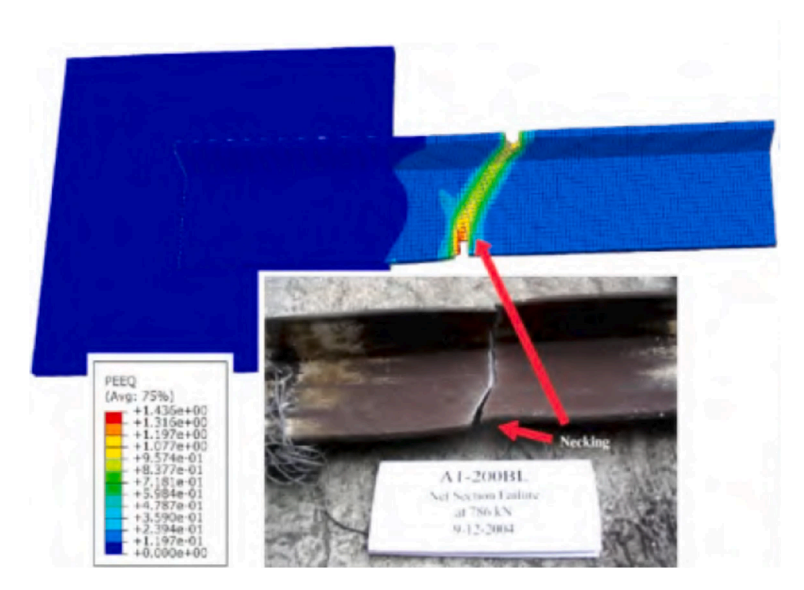


Fig. 13. Comparison of FE results and experimental observation, fractured profile of Specimen L1.

**Table 2**Single and double channel connection FE models.

Specimen No.	Specimen ID	Channel section	Weld length, l <sub>w</sub> (mm)	Gusset thickness, t <sub>gp</sub> (mm)	Weld size, a <sub>w</sub> (mm)
1	U60-50-8-6	UNP60	50	8	6
2	U100-80-8-6	UNP100	80	8	6
3	U160-100-8-6	UNP160	100	8	6
4	U200-150-12-10	UNP200	150	12	10
5	2U160-110-25-12	2UNP160	110	25	12
6	2U200-150-40-12	2UNP200	150	40	12
7	2U300-200-40-16	2UNP300	200	40	16
8	2U400-300-40-20	2UNP400	300	40	20

axis depicts the elongation along the length of the member. Detailed description is given below.

#### 5.3.1. Monotonic loading

The load-displacement curves for single channel members (models 1–4) under monotonic loading are shown in Fig. 20. As illustrated, prior to reaching approximately 85 % of the maximum tensile strength, the load-displacement curves for all models subjected to monotonic tensile and compressive forces exhibit a similar trend. Subsequently, beyond this point, the data indicates that in all models with single-channel member, the compression capacity is greater than tension capacity. The average ratio of maximum compressive to tensile capacity for these models were 1.16. Moreover, the load-displacement curves for tension and compression significantly diverge from each other after the aforementioned point and under compression more ductile behaviour is observed.

In Fig. 20 comparison is also made against AISC equations for SY and SR strengths. The FE analyses demonstrated that the  $SY_{FEM}$  exhibited a reduction of between 24.5 and 28.9 % compared to the recommended  $SY_{AISC}$  (Eq. (2)). This can be attributed to the conservative way the yield strength was determined from the load-displacement curves in this study, which was based on the end of linear portion of the curve. However, for both tensile and compressive loading, the maximum shear rupture strength values obtained from the FE analyses (SR\_{FEM}) were larger than the SR\_{AISC} (Eq. (3)). This means the AISC equations are safe to use for tensile loading and more so for compressive loading.

The load-displacement curves for double-channel members (models 5–8) under monotonic loading are shown in Fig. 21. In these models, the curves exhibited a similar pattern under both types of loading until reaching approximately the peak tensile strength. The ratio between the maximum compressive and tensile strengths (SR) for the smallest specimen is approximately 1.1, while it decreases to 0.97 for the largest specimen. This indicates that for large channel sizes under compressive loading a reduction in compressive strength relative to tensile strength might occur due to local instability. The figure shows that, similar to the single-channel members, all SR<sub>FEM</sub> values are larger than SR<sub>AISC</sub> values, while SY<sub>FEM</sub> values are less than SY<sub>AISC</sub>. Therefore, the AISC overestimates the SY values, while the SR<sub>AISC</sub> results are on the safe side.

#### 5.3.2. Cyclic loading

Fig. 22 illustrates the load-displacement curves of single-channel members (models 1-4) subjected to cyclic loading. The positive values on the vertical axis indicate shear strength under tensile loading, while the negative values correspond to strength under compressive loads. The figure illustrates that under cyclic loading, the maximum capacities are approximately equal under tension and compression. This observation is analogous to the results of Fig. 20, where for small displacements, models exhibited approximately equal strength under tension and compression. As shown, the damage has initiated at significantly smaller displacements, and the total rupture has occurred much sooner under cyclic loading as compared to monotonic loading. This demonstrates that under cyclic loading, the shear strength of the brace members experiences a notable decline. In addition, the figure illustrates that under cyclic loading, the strength has decreased around 11.7 to 16.3 % as compared to monotonic tension and 30.3 to 33.3 % as compared to monotonic compressive loading. It is seen that in all cases the AISC shear rupture strength predictions are very close to FE results.

Fig. 23 depicts load-displacement curves for double-channel members (models 5–8). As seen, under cyclic loading, the maximum capacities are approximately equal under tension and compression, consistent with observations made for single-channel members. Additionally, the  $SR_{FEM}$  values are decreased under cyclic loading compared to models under monotonic loading. As with single-channel members, after reaching the maximum capacity, the specimens lose their entire strength after ultimately five cycles. The results show that the discrepancies between  $SR_{FEM}$  and  $SR_{AISC}$  values are very low.

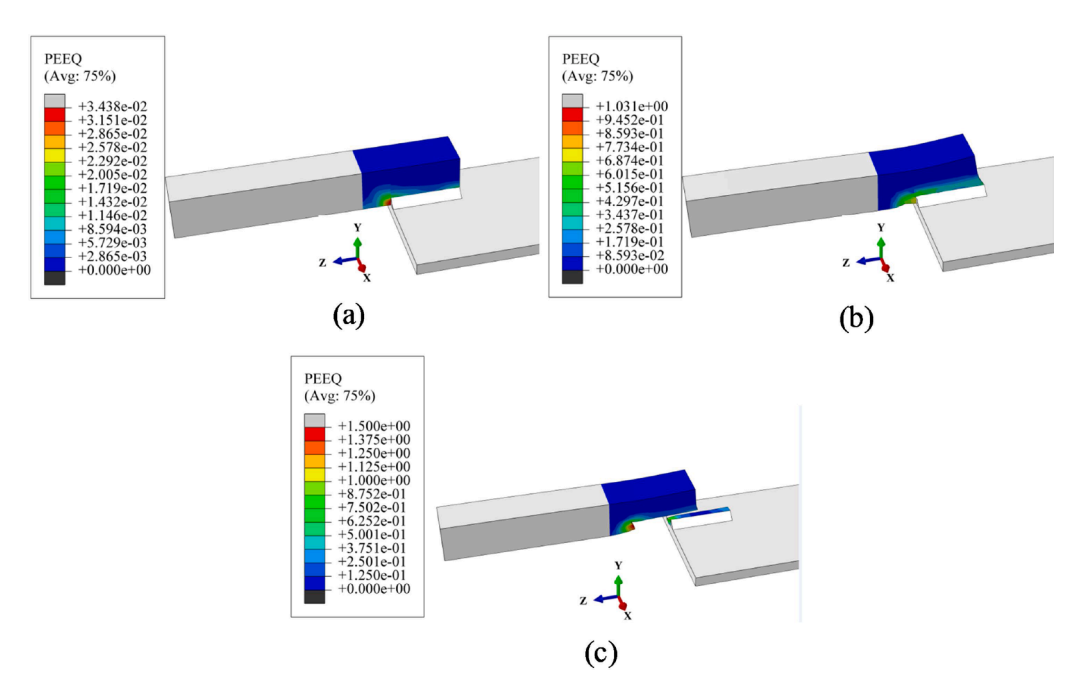


Fig. 14. The rupture mode of U60-50-8-6 model under uniform tension at the (a) SY, (b) SR limit load and (c) final rupture.

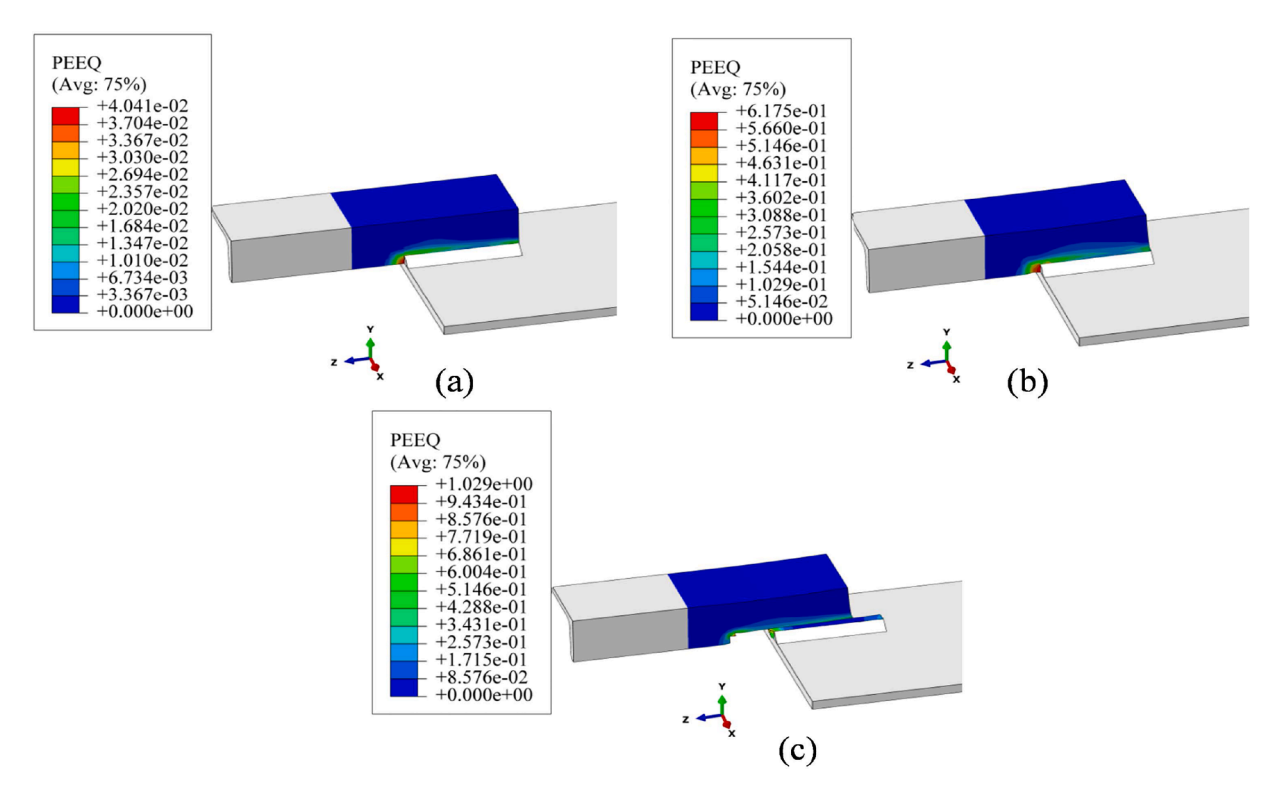


Fig. 15. The rupture mode of 2U160-110-25-12 model under uniform tension at the (a) SY, (b) SR limit load and (c) final rupture.

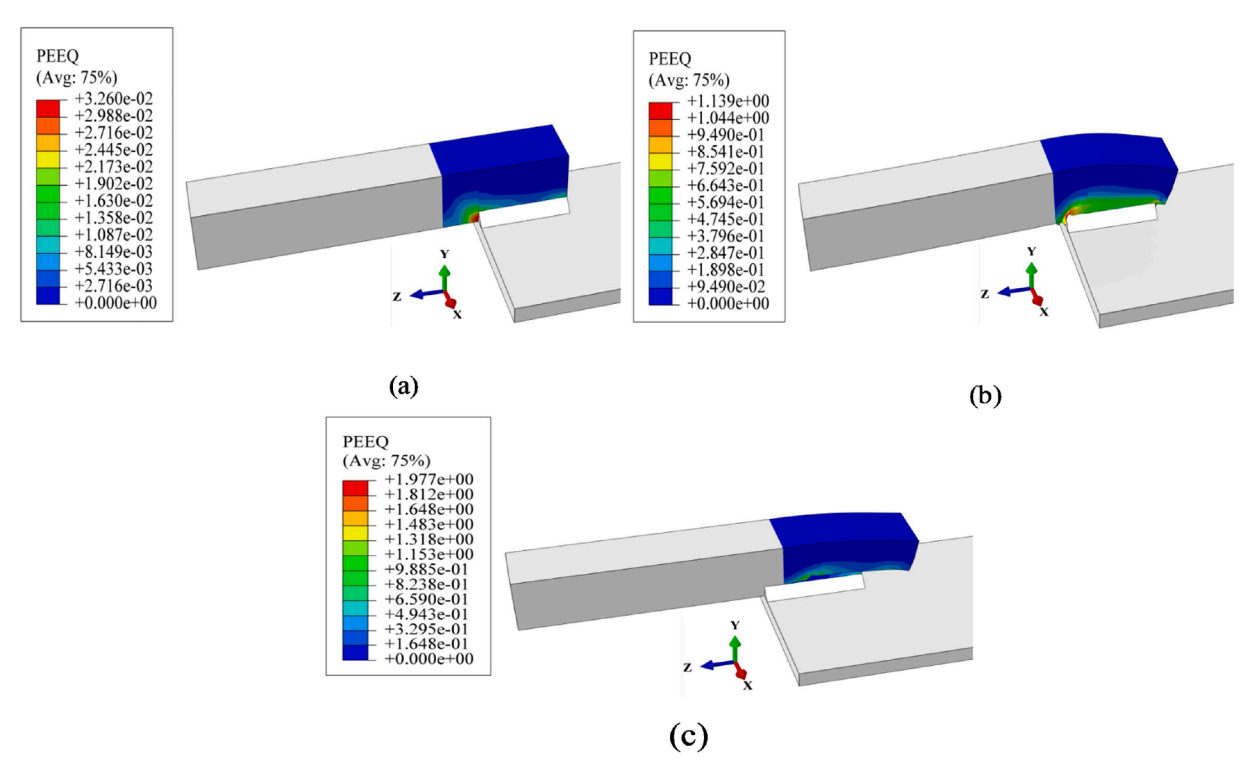


Fig. 16. The rupture mode of U60-50-8-6 model under uniform compression at the (a) SY, (b) SR limit load and (c) final rupture.

## 5.3.3. Results summary

Finally, the results of the FE analyses are compared with the AISC values in Table 3. The average ratios of SRFEM/SRAISC are 1.13 and 1.24 for monotonic tension and compression, respectively, confirming that AISC predictions are generally conservative. In contrast, the average ratio of SYFEM/SYAISC is 0.81 for both loading types. This

discrepancy arises from the conservative procedure used to define shear yield in this study, where SY was identified at the end of the linear portion of the load—displacement curve. Since SY is not a failure limit state but rather a deformation threshold, the lower FE estimates are not a concern in most cases where yield displacements are acceptable, and the AISC values remain safe for design.

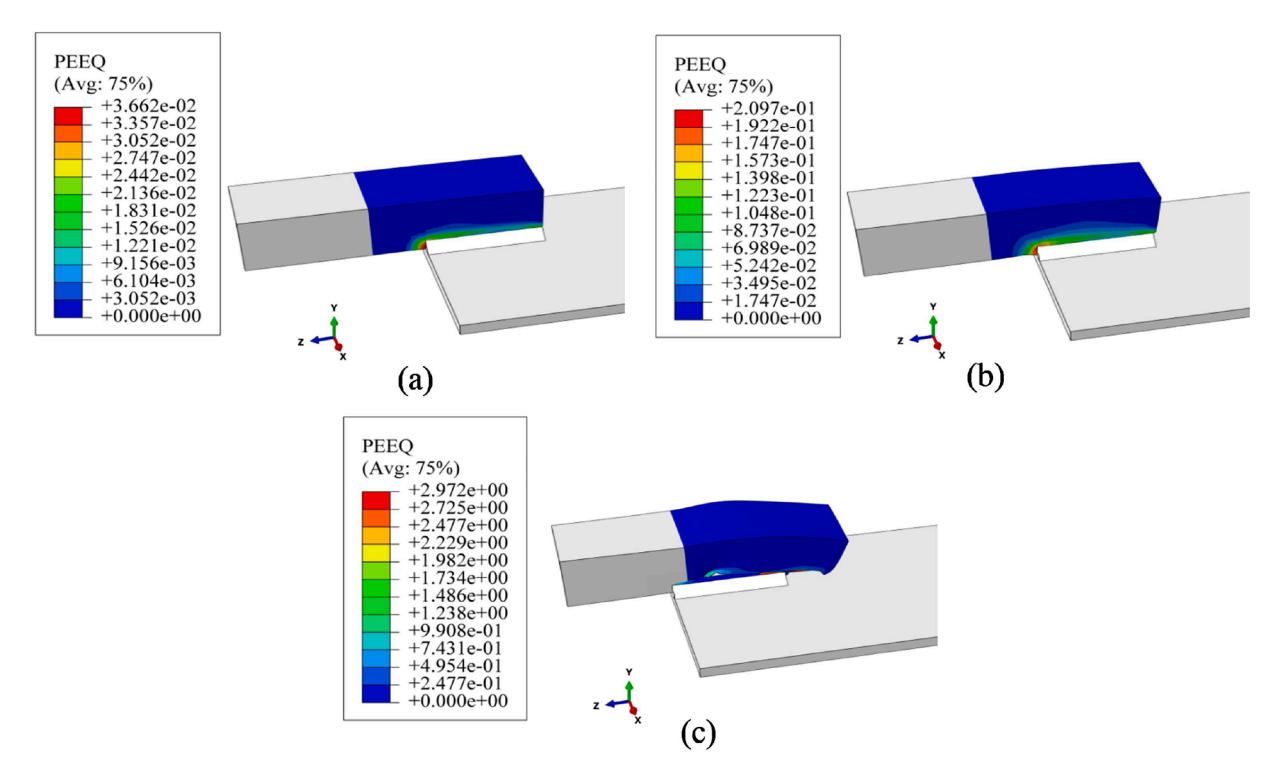


Fig. 17. The rupture mode of 2U160-110-25-12 model under uniform compression at the (a) SY, (b) SR limit loads and (c) final rupture.

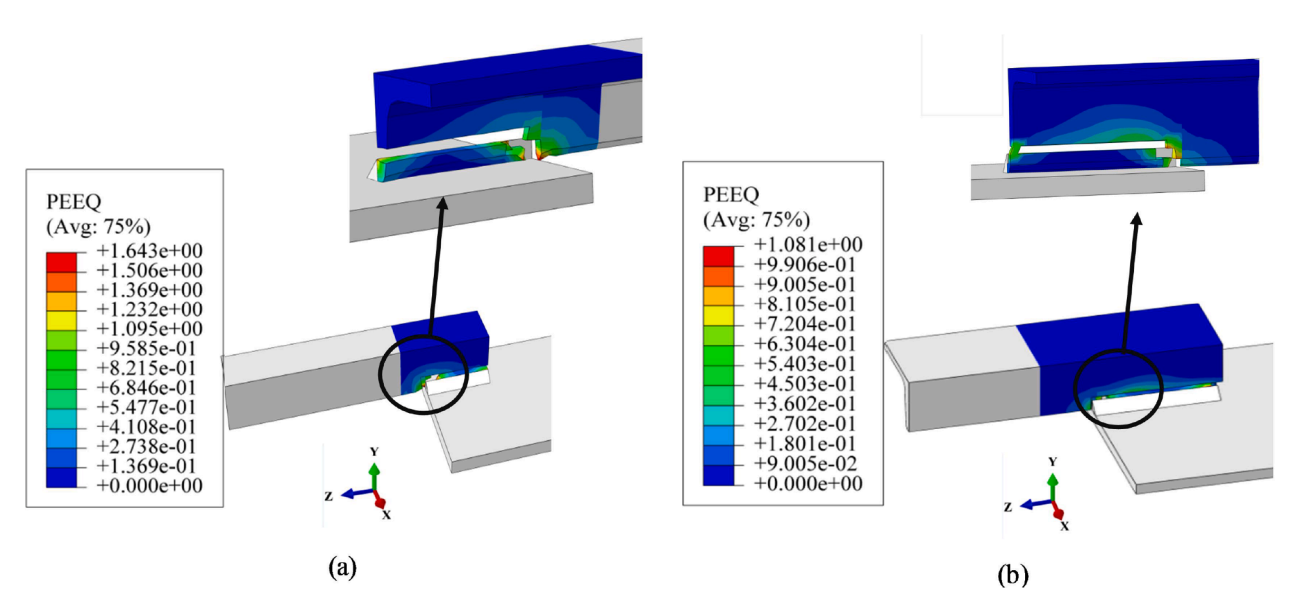


Fig. 18. The final rupture modes of (a) U60-50-8-6 and (b) 2U160-110-25-12 model under cyclic loading.

A clear size-dependent trend is also observed. For both single- and double-channel members, the SRFEM/SRAISC ratio decreases as member size increases: under monotonic tension, it falls from approximately 1.25 for the smallest section to about 1.06 for the largest, while under monotonic compression it reduces from about 1.47 to 1.08. Similar trends appear under cyclic loading, although the absolute strengths are lower than under monotonic loading due to adverse cyclic effects such as low-cycle fatigue and local buckling. Although a detailed fatigue-life assessment is beyond the scope of this study, the observed reduction in cyclic strength is consistent with low-cycle fatigue mechanisms associated with repeated plastic straining and weld toe stress concentration. The progressive PEEQ localization observed in the cyclic simulations qualitatively reflects damage accumulation and stiffness

degradation typical of fatigue-type behavior, confirming that the adopted ductile-damage model captures the essential aspects of cyclic degradation relevant to welded channel–gusset connections. On average, FE cyclic SR results are only about 3 % higher than AISC predictions, but for the largest single-channel members the AISC check slightly overestimates the SR capacity. Overall, these results demonstrate that the AISC shear-rupture equation is consistently conservative, with conservatism diminishing for larger members, while SY predictions are lower than AISC estimates by about 68 % on average—relevant only in cases where excessive deformation cannot be tolerated.

Nevertheless, it should be acknowledged that in rare cases where deformation control governs design—such as in brace systems subjected to severe cyclic drift demands—the discrepancy in SY predictions may

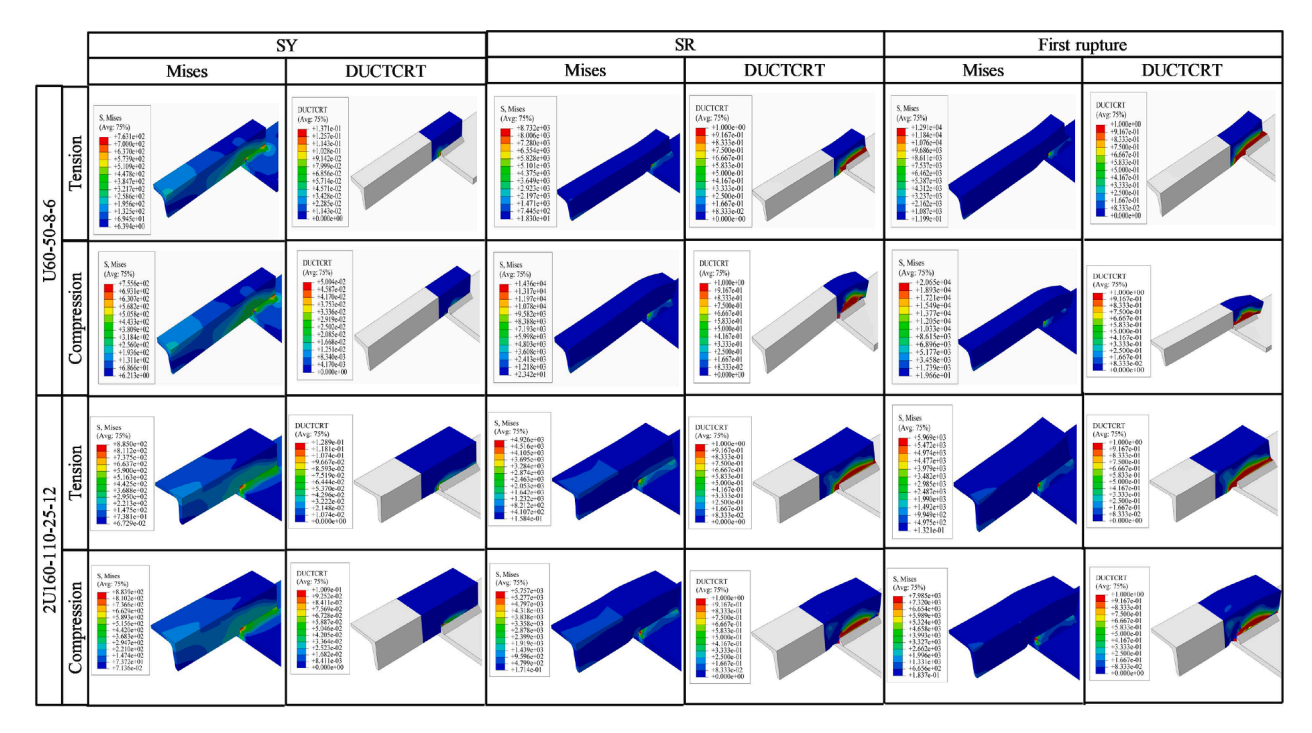


Fig. 19. Von-Mises contours and DUCTCRT of the smallest single and double channel sections.

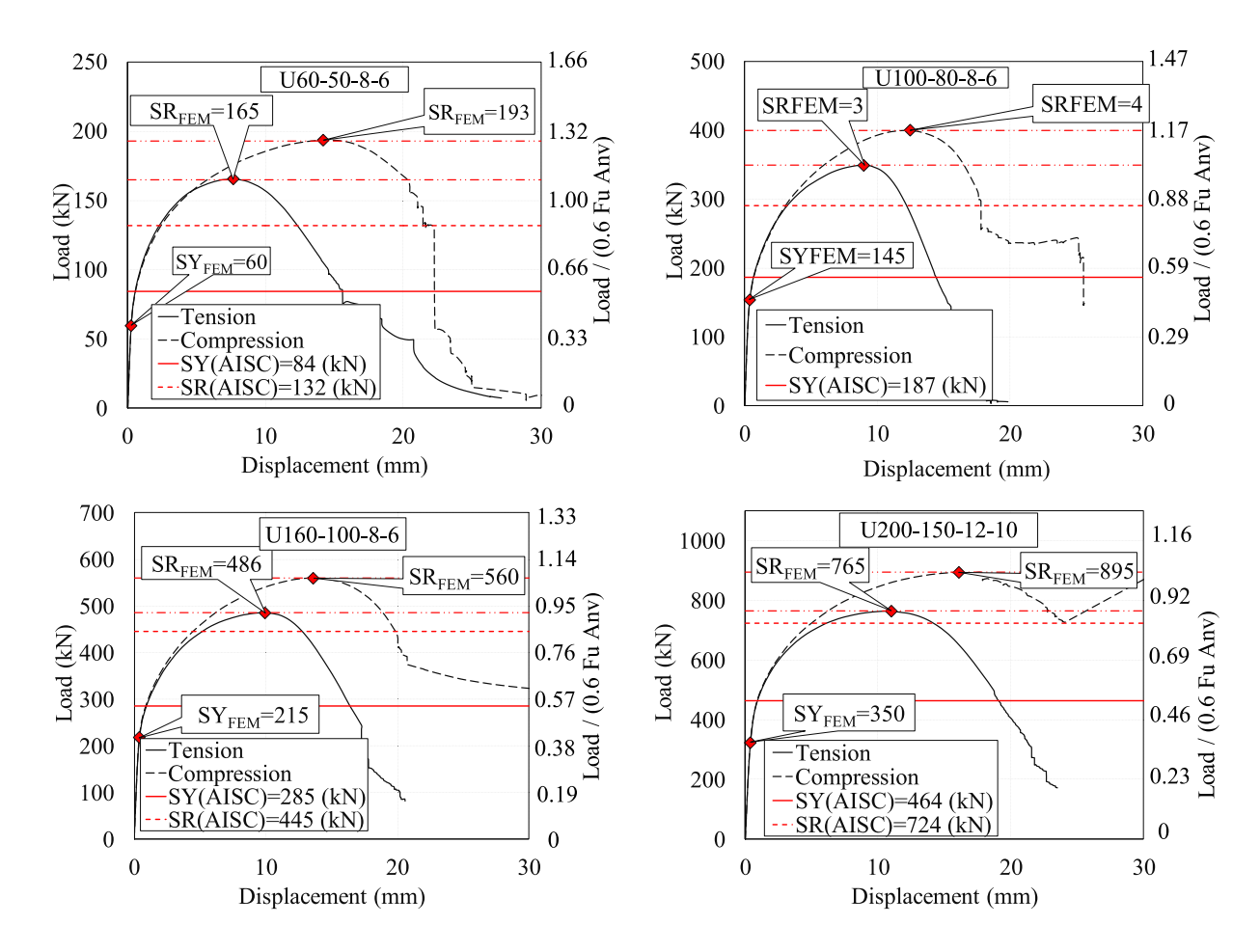


Fig. 20. Load- displacement curves for specimens with single channel members under monotonic loading.

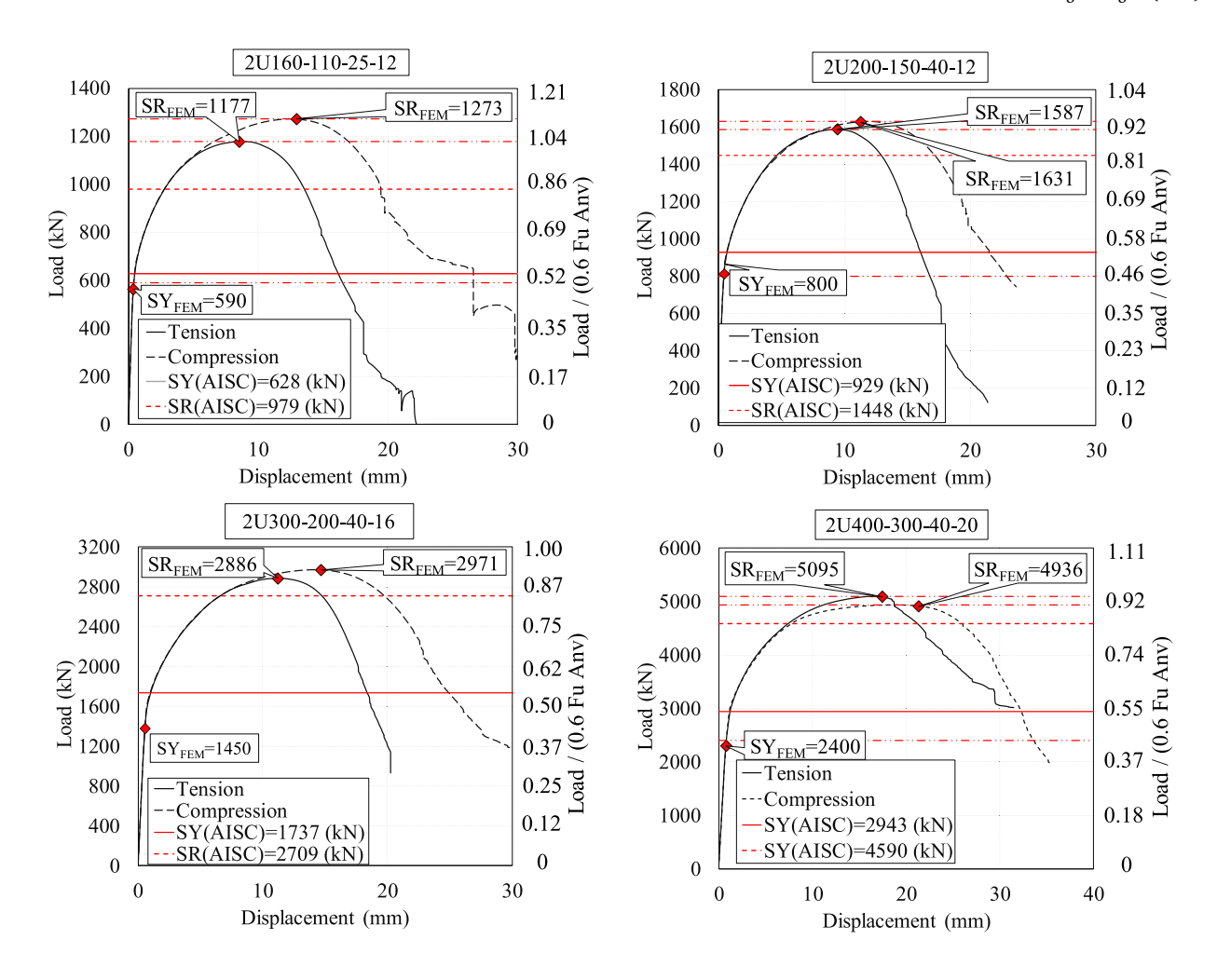


Fig. 21. Load- displacement curves for specimens with double channel members under monotonic loading.

become relevant. In such situations, SY should be explicitly checked in addition to SR, whereas in conventional strength-controlled design the governing rupture limit state ensures safety.

To investigate the observed significant decrease in the compression-to-tension SR ratio, additional PEEQ contour plots under compressive loading near the SR stage were extracted for the smallest and largest double-channel specimens (Fig. 24). The largest section shows strongly out-of-plane distortion in its flange near the gusset interface, indicative of emerging local buckling. This localization explains why the compression-to-tension SR ratio decreases toward unity ( $\approx 0.97$ ) with increasing member size, marking a threshold where local instability begins to reduce compressive strength relative to tension.

To generalize the observed behavior beyond the specific UNP sizes, the strength ratios were also re-expressed in terms of non-dimensional geometric parameters: gusset weld length to flange thickness (lw/tf), gusset plate thickness to flange thickness (tgp/tf), weld size to flange thickness (aw/tf), and a flange slenderness index. Fig. 25 presents the variation of SR<sub>FEM</sub>/SR<sub>AISC</sub> with these parameters. The red markers show single-channel members and blue markers show double-channel members. The plots confirm that for relatively stocky sections (low slenderness and smaller lw/tf), the AISC shear rupture provisions are more conservative, with ratios exceeding unity. As flange slenderness and relative gusset proportions increase, the ratios approach unity and even

less, indicating that the conservatism of AISC predictions diminishes. Additionally, an increase in aw/tf ratio causes more conservative results of AISC predictions. The non-dimensional representation thus highlights threshold regimes where geometric effects become critical, providing more portable design insight than raw section sizes.

To examine the sensitivity of shear yielding (SY) to its definition, additional analyses were performed using the tangent modulus criterion with a stiffness reduction threshold of 50 % (see Table 4). The resulting SY values were generally close to those obtained with the end-of-linear method, with most specimens showing only minor differences, confirming that the observed shortfall of SYFEM relative to SYAISC is not merely a methodological artifact. Instead, it reflects a consistent trend in which finite element models predict lower deformation-controlled strengths than the code equations.

## 5.3.4. The effects of increase in weld length on the models

It is well known that longer length welds increase the SR capacity of the braces. This in turn can change the failure mode to tension rupture (TR) limit state in the brace connection area. In order to examine the effect of weld length on the models, the double-channel members were selected for this investigation. The weld lengths in models 5 to 8 were increased to 250, 310, 400, and 550 mm, respectively. Fig. 26 illustrates the ultimate failure path of the models under various loading conditions.

S. Maleki et al. Results in Engineering 28 (2025) 108448

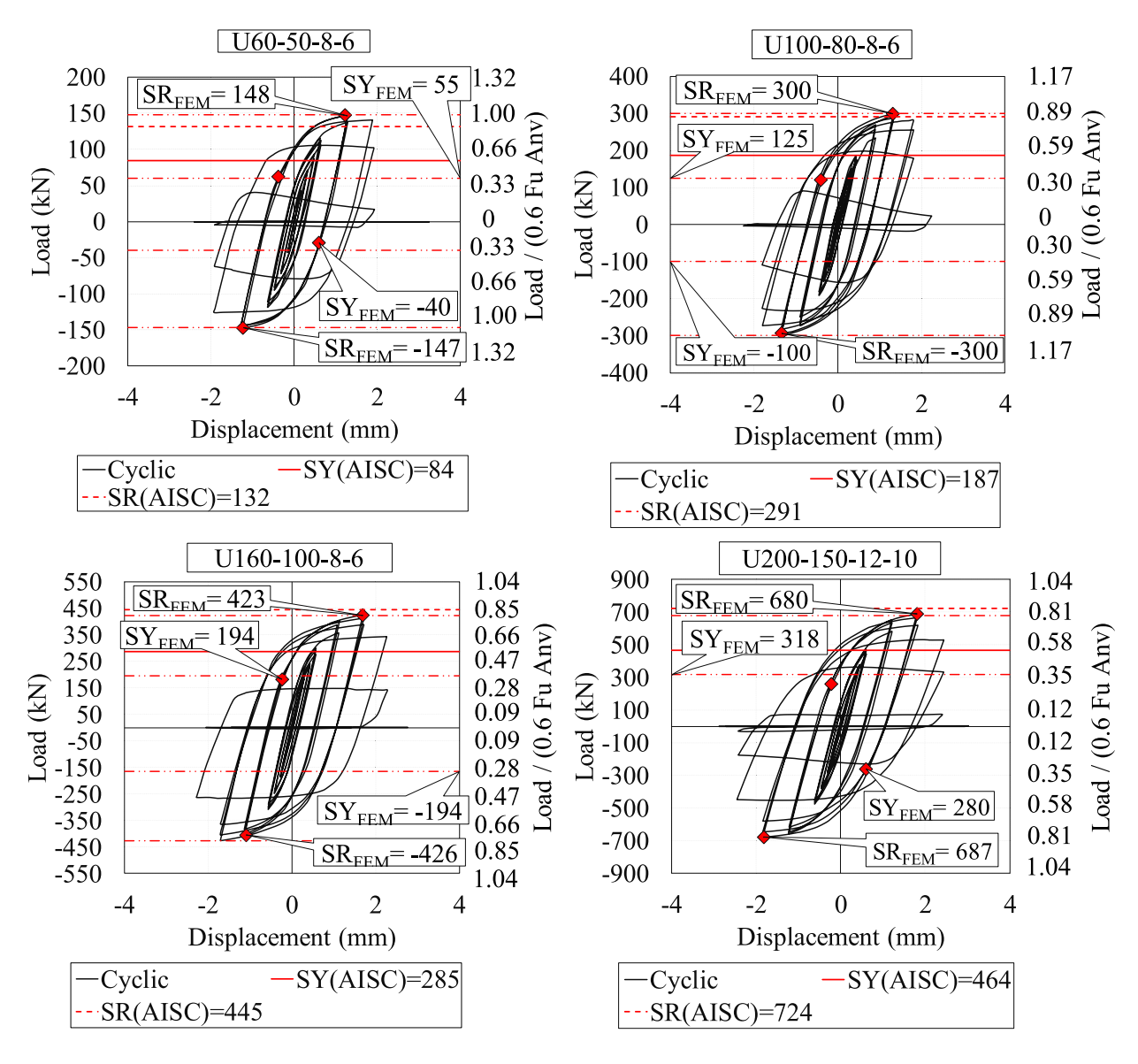


Fig. 22. Load- displacement curves for specimens with single-channel members under cyclic loading.

Under monotonic tensile and compressive loading, a tension rupture (TR) was observed. The rupture path progresses in a perpendicular direction to the length of the weld until the structure is entirely ruptured. As expected, when the weld lengths were increased, the shear rupture (SR) was eliminated in all models. In models under cyclic loading, the rupture path did not propagate by a shear or tension pattern and exhibits a distinct pattern. The rupture originates from the intersection of the channel and gusset edge, where there is a high stress concentration. In the smallest specimen, the rupture propagated around the flange of the member at a relative angle of 65 degrees with respect to the weld direction. After reaching the web of the channel, the rupture continued perpendicular to the load direction. In larger models, the rupture path in the flange of the channel propagated with smaller slopes, yet the total shape of rupture remains analogous to that observed in the smallest model. In the largest model, the rupture path in the flange was at 45 degrees with respect to the weld direction.

The peak tensile strength of the models with larger weld and channel lengths under different types of loading are compared with AISC provisions in Table 5. It is seen that the AISC tension rupture values which includes the shear lag factor (U) is on the conservative side and safe to use in all cases.

## 5.3.5. Analytical regression model for SR prediction

To enhance the analytical interpretation of the results and generalize the findings beyond the tested configurations, a multivariate regression model was developed to predict the shear rupture ratio  $SR_{FEM}/SR_{AISCS}$  as a function of key geometric and loading parameters. Seven independent variables were considered: number of channels (X1), UNP size (X2), weld length (X3), weld thickness (X4), gusset plate thickness (X5), loading type (X6; monotonic = 0, cyclic = 1), and loading direction (X7; tension = 0, compression = 1). The resulting 15-term polynomial regression achieved a mean absolute percentage error (MAPE) of 1.8 %

S. Maleki et al. Results in Engineering 28 (2025) 108448

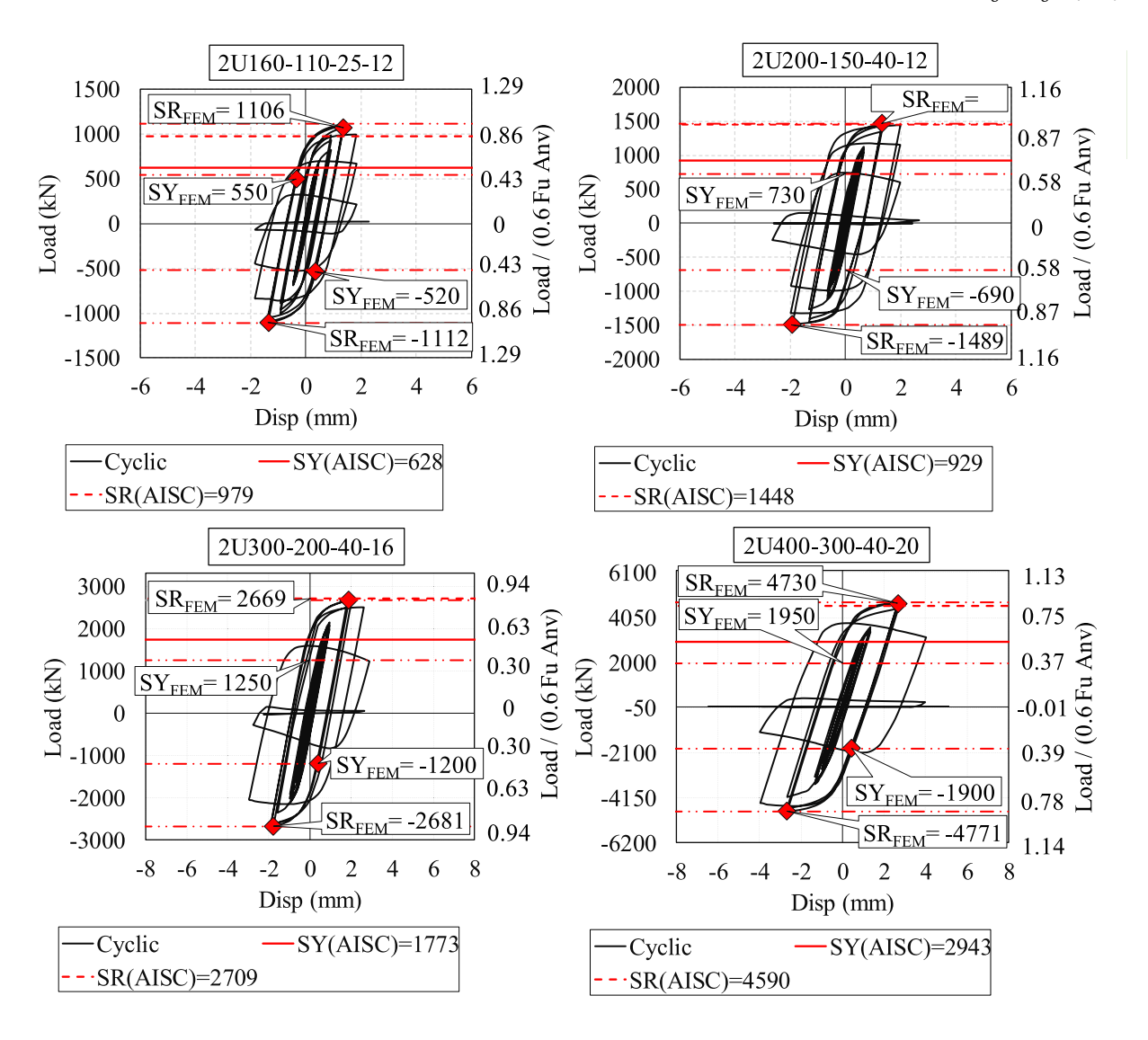


Fig. 23. Load- displacement curves for specimens with double channel members under cyclic loading.

and maximum error <4 percent, indicating excellent predictive capability. The simplified predictive equation is expressed as:

#### 6. Conclusions

The SY and SR limit states in welded single and double-channel members under monotonic and cyclic loadings were investigated using

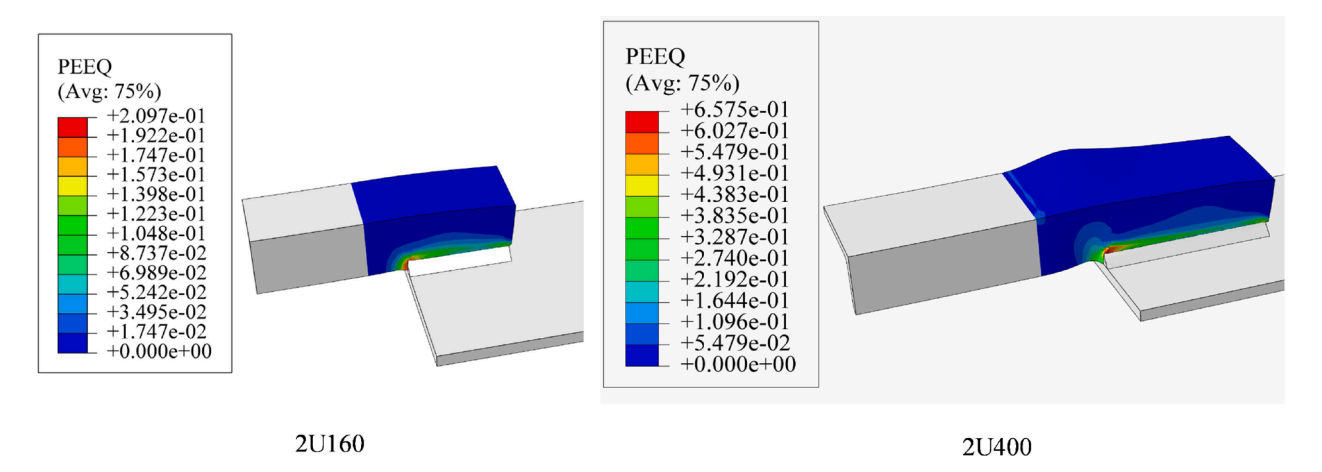
$$SR \ (\textit{ratio}) = 1.36199 \ + \ 0.0966121 \ * \ \textit{X}(2) \ * \ \textit{X}(6) \ - \ 0.10375 \ * \ \textit{X}(6) \ * \ \textit{X}(7) \ + \ 0.0983368 \ * \ \textit{X}(7)^2 \ - \ 0.0653181 \ * \ \textit{X}(2) \ * \ \textit{X}(7) \ - \ 0.0632369 \ * \ \textit{X}(6)^2 \ + \ 0.0327789 \ * \ \textit{X}(7) \ - \ 0.021079 \ * \ \textit{X}(6) \ + \ 0.00411283 \ * \ \textit{X}(5) \ * \ \textit{X}(7) \ + \ 0.00553378 \ * \ \textit{X}(5) \ * \ \textit{X}(6) \ - \ 0.00157805 \ * \ \textit{X}(1) \ - \ 0.000438971 \ * \ \textit{X}(3) \ * \ \textit{X}(7) \ + \ 0.000118886 \ * \ \textit{X}(1)* \ \textit{X}(2) \ - \ 0.000198438 \ * \ \textit{X}(4)^2 \ + \ 4.95682e \ - \ 05 \ * \ \textit{X}(3) \ * \ \textit{X}(4) \ - \ 0.00032208 \ * \ \textit{X}(3)$$

The model shows that the interaction between UNP size, loading type, and direction (X2  $\times$  6, X6  $\times$  7, X2  $\times$  7) has the most significant influence on SR prediction, confirming that both geometric scaling and loading regime jointly affect rupture behavior. The regression thus provides a compact yet accurate analytical framework that can assist designers in quickly estimating the expected deviation of AISC shear-rupture predictions for welded channel–gusset configurations.

nonlinear finite element models. The modelling technique and the assumptions adopted were validated through comparison with similar tested specimens. Aiming to capture the real failure pattern in channel members, as well as the full-range load-displacement response, a stress-triaxiality dependent fracture criterion accompanied with progressive damage evolution option in Abaqus, were employed. Thereafter, an extensive parametric study was performed considering channel members with various sizes, connection lengths, gusset plate thicknesses, and

Table 3
Results summary.

Type of loading	Specimen ID	SR <sub>FEM</sub> (kN)	SR <sub>AISC</sub> (kN)	$SR_{FEM}/SR_{AISC}$	Error %	SY <sub>FEM</sub> (kN)	SY <sub>AISC</sub> (kN)	$SY_{FEM}/SY_{AISC}$	Error %	$\Delta_{\mathrm{y}}$	Cycles
Monotonic tension	U60-50-8-6	165	132	1.25	20.00	60	84	0.71	-40.00	0.26	
	U100-80-8-6	349	291	1.20	16.62	145	187	0.78	-28.97	0.45	
	U160-100-8-6	486	445	1.09	8.44	215	285	0.75	-32.56	0.57	
	U200-150-12-10	765	724	1.06	5.36	350	464	0.75	-32.57	0.61	
	2U160-110-25-12	1177	979	1.20	16.82	590	628	0.94	-6.44	0.48	
	2U200-150-40-12	1587	1448	1.10	8.76	800	929	0.86	-16.13	0.67	
	2U300-200-40-16	2886	2709	1.07	6.13	1450	1737	0.83	-19.79	0.95	
	2U400-300-40-20	5095	4590	1.11	9.91	2400	2943	0.82	-22.63	1.20	
	STDEV			0.071				0.073			
	Average:			1.13				0.81			
Monotonic compression	U60-50-8-6	193	132	1.47	31.61	60	84	0.71	-40.00		
•	U100-80-8-6	400	291	1.37	27.25	145	187	0.78	-28.97		
	U160-100-8-6	560	445	1.26	20.54	215	285	0.75	-32.56		
	U200-150-12-10	895	724	1.24	19.11	350	464	0.75	-32.57		
	2U160-110-25-12	1273	979	1.30	23.10	590	628	0.94	-6.44		
	2U200-150-40-12	1631	1448	1.13	11.22	800	929	0.86	-16.13		
	2U300-200-40-16	2971	2709	1.10	8.82	1450	1737	0.83	-19.79		
	2U400-300-40-20	4936	4590	1.08	7.01	2400	2943	0.82	-22.63		
	STDEV			0.137				0.073			
	Average:			1.24				0.81			
Cyclic loading (tension)	U60-50-8-6	148	132	1.12	10.81	55	84	0.65	-52.73		24
-)	U100-80-8-6	300	291	1.03	3.00	125	187	0.67	-49.60		21
	U160-100-8-6	423	445	0.95	-5.20	194	285	0.68	-46.91		18
	U200-150-12-10	680	724	0.94	-6.47	318	464	0.69	-45.91		20
	2U160-110-25-12	1112	979	1.14	11.96	550	628	0.88	-14.18		18
	2U200-150-40-12	1468	1448	1.01	1.36	730	929	0.79	-27.26		17
	2U300-200-40-16	2669	2709	0.99	-1.50	1250	1737	0.72	-38.96		18
	2U400-300-40-20	4730	4590	1.03	2.96	1950	2943	0.66	-50.92		15
	STDEV			0.072				0.079			
	Average:			1.03				0.72			
Cyclic loading (compression)	U60-50-8-6	147	132	1.12	10.20	40	84	0.48	-110.00		24
· r · · · · ·	U100-80-8-6	300	291	1.03	3.00	100	187	0.53	-87.00		21
	U160-100-8-6	426	445	0.96	-4.46	165	285	0.58	-72.73		18
	U200-150-12-10	687	724	0.95	-5.39	280	464	0.60	-65.71		20
	2U160-110-25-12	1106	979	1.13	11.48	520	628	0.83	-20.77		18
	2U200-150-40-12	1489	1448	1.03	2.75	690	929	0.74	-34.64		17
	2U300-200-40-16	2681	2709	0.99	-1.04	1200	1737	0.69	-44.75		18
	2U400-300-40-20	4771	4590	1.04	3.79	1900	2943	0.65	-54.89		15
	STDEV			0.066				0.114	,		
	Average:			1.03				0.64			



 $\textbf{Fig. 24.} \ \ \textbf{The PEEQ of 2U160-110-25-12 model under uniform compression at the SR limit load}.$ 

weld leg sizes. The effects of these parameters on the SY and SR strengths of channel brace members were studied, and the failure paths were determined. Based on the analytical and numerical efforts involved in this research, the subsequent conclusions can be drawn:

 The rupture paths observed under monotonic and cyclic loading for single and double channel members were notably similar. However, under compressive loading, rupture occurs at higher displacement levels. The failure initiates in the small tension region where the member connects to the edge of the gusset plate. Subsequently, the crack propagates along the channel flange, nearly parallel to the

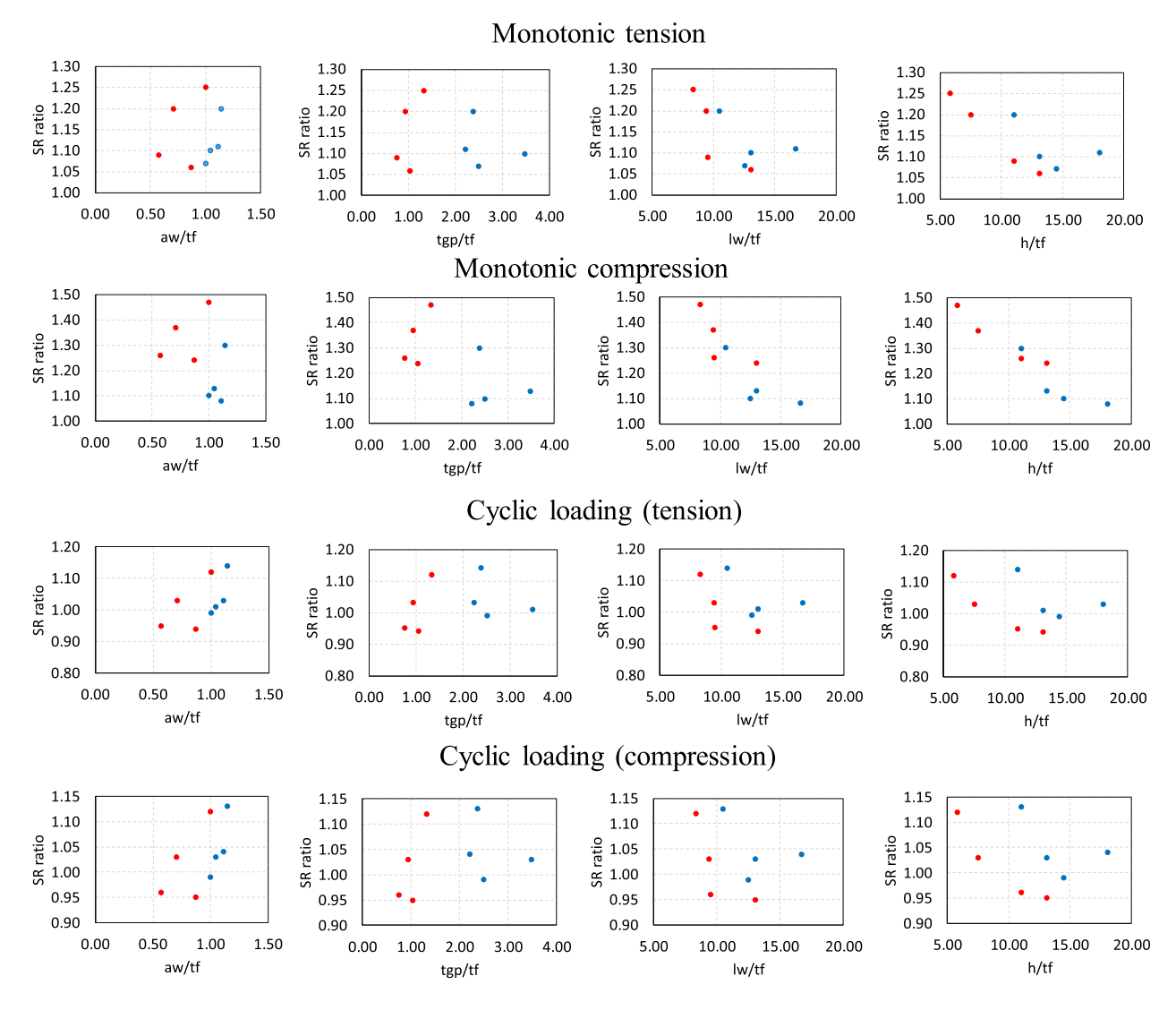


Fig. 25. The effects of non-dimensional parameters on SR ratios.

**Table 4**The results of SY values with different methods.

Type of loading	Specimen ID	SY (tangent- modulus criterion)	SY (end of the linear portion)	Error %
Monotonic	U60-50-8-6	74	60	19.7
tension	U100-80-8-6	150	145	3.7
	U160-100-8-6	214	215	-0.7
	U200-150-12-10	322	350	-8.8
	2U160-110-25-12	653	590	9.7
	2U200-150-40-12	844	800	5.3
	2U300-200-40-16	1544	1450	6.1
	2U400-300-40-20	3026	2400	20.6

longitudinal welds. Therefore, the shear area for AISC equations (Eqs. 2&3) are conservative to use. In members with longer weld lengths, the rupture mode transitions from shear rupture to tension rupture, as anticipated. The crack in the flange extends into the channel web in a direction perpendicular to the applied load.

The average ratio of shear rupture strength from FE analyses to that
predicted by the AISC equation (SR<sub>FEM</sub>/ SR<sub>AISC</sub>) under monotonic
tension is 1.13, increasing to 1.24 under monotonic compression.
Thus, the AISC equation provides a conservative prediction of shear

rupture capacities under monotonic loading, particularly under compressive conditions. Note that the addition of strength reduction factor of 0.75 in design of these members increases the reliability index even further.

- Under monotonic tensile and compressive loading, the average ratio
  of SY<sub>FEM</sub>/ SY<sub>AISC</sub> is 0.81. This discrepancy arises from the conservative method employed in this study to measure shear yield values.
  The SY values were determined at the end of the linear portion of the
  load-displacement curves. It is important to note that the SY limit
  state does not lead to complete failure but rather causes excessive
  deformation. As a result, the AISC values remain appropriate and
  safe for most cases where yield displacements are acceptable.
- The application of cyclic loading results in a significant reduction in the average ratios of SR<sub>FEM</sub>/ SR<sub>AISC</sub>. This decrease is primarily driven by the combined influence of low-cycle fatigue and local buckling. The average ratio of SR<sub>FEM</sub>/ SR<sub>AISC</sub> for models under cyclic loading is 1.03. This indicates that the AISC equations overall provide accurate predictions of shear rupture strength in these scenarios. Consequently, they can be confidently applied in practice. Note that the addition of strength reduction factor of 0.75 in design of these members ensures reliability.
- ullet For models with larger weld lengths, shear rupture no longer governs strength. The average TR<sub>FEM</sub>/ TR<sub>AISC</sub> ratios are 1.13 for monotonic

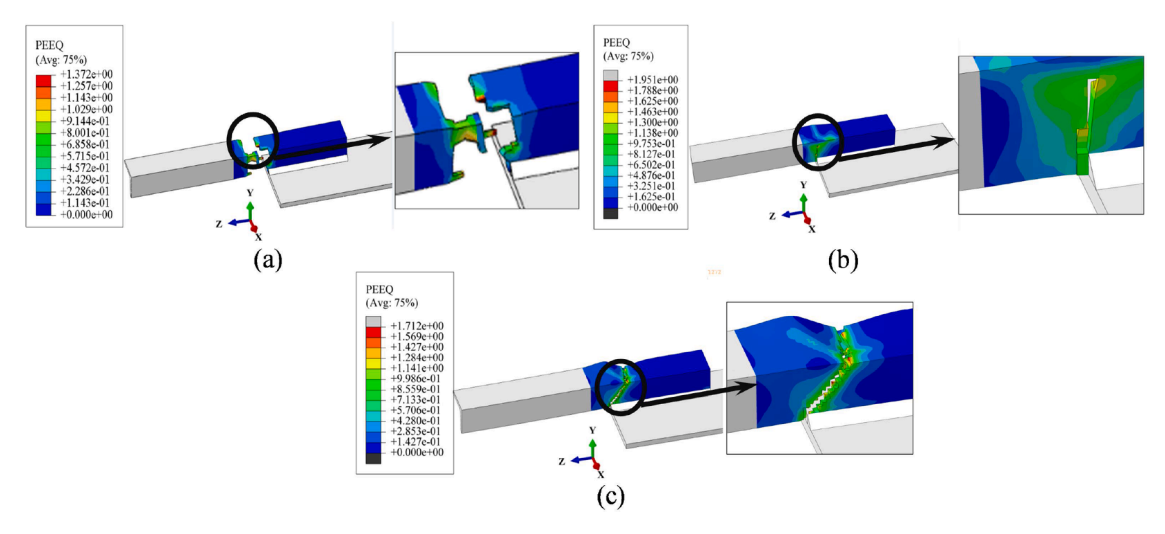


Fig. 26. The rupture mode of 2U160-250- 25-12 model at the final stage under (a) monotonic tensile, (b) monotonic compressive and (c) cyclic loading.

Table 5
Results summary for extended weld length.

,		U			
Type of loading	Specimen ID	TR <sub>FEM</sub> (kN)	U	TR <sub>AISC</sub> (kN)	${\rm TR}_{\rm FEM}/$ ${\rm TR}_{\rm AISC}$
Monotonic tension	2U160-250-25-12	1889	0.81	1628	1.16
	2U200-310-40-12	2519	0.82	2212	1.14
	2U300-400-40-16	4510	0.81	3992	1.13
	2U400-550-40-20	7008	0.85	6475	1.08
	Average:				1.13
Cyclic loading (tension)	2U160-250-25-12	2040	0.81	1628	1.25
	2U200-310-40-12	2656	0.82	2212	1.20
	2U300-400-40-16	4739	0.81	3992	1.19
	2U400-550-40-20	7160	0.85	6475	1.11
	Average:				1.19

loading and 1.19 for cyclic loading. These results confirm that the AISC tension rupture formula and the shear lag factor are reliable and safe for the scenarios considered.

- The study highlights that while the AISC shear rupture provisions are
  consistently conservative across all cases studied, the finite element
  results indicate that shear yielding capacities may be on average 68
  % lower than the AISC estimates. This discrepancy is not critical in
  strength-controlled designs where rupture governs, but it may be
  significant in deformation-controlled scenarios, such as brace systems subjected to severe cyclic drift demands. Designers should
  therefore be cautious when SY displacement demands are likely to
  control system performance.
- The hysteretic parameters obtained in this work—stiffness degradation, pinching indices, and equivalent viscous damping—provide practical input values for nonlinear seismic analyses and macromodel calibration. These results can support practicing engineers and code developers in refining performance-based seismic design checks for welded channel brace connections.
- While the present study provides valuable insights into the cyclic behavior of welded single- and double-channel brace connections, it should be recognized that most of the results are derived from finite element simulations. Apart from the validation against available test data, the broader parametric trends have not yet been experimentally verified. Future studies incorporating targeted experimental testing would therefore be essential to confirm and extend the numerical findings presented here.
- The practical implications of this study have direct relevance for engineering design and seismic assessment of braced steel frames.

First, the quantified shear yielding (SY) and shear rupture (SR) strengths under cyclic loading provide more realistic capacity values than current AISC provisions, which were found in some cases to be unconservative. Second, the observed cyclic strength degradation ( $\approx$ 15 % in tension and  $\approx$ 30 % in compression) highlights the need to incorporate degradation models in performance-based seismic design, rather than relying only on monotonic strengths. Third, the hysteretic parameters reported in this study—secant stiffness degradation, pinching indices, equivalent viscous damping, and cumulative plastic deformation—can be directly used in nonlinear time-history analyses and in calibrating simplified brace connection models for structural simulations. Finally, the validated FE framework offers a practical and computationally efficient tool that engineers and researchers can extend to other brace geometries, connection details, and loading protocols, thereby supporting safer and more economical seismic design of steel braced systems.

- To support practical application of the findings, a regression-based predictive formula was developed to estimate the finite element shear rupture strength as a function of the governing geometric and loading parameters. The proposed expression can be used as a modification factor to AISC shear-rupture provisions for welded channel–gusset connections, offering improved accuracy with a maximum error below 4 %. This equation enables engineers to rapidly approximate the finite-element-based capacity without detailed numerical analysis, thereby enhancing the practical usability of the study's results.
- The modeling framework incorporates several idealizations: tie constraints were used to represent welds, the gusset plate was restrained in-plane, and residual stresses, weld discontinuities, and micromechanical fatigue effects were not explicitly modeled. Sensitivity analyses on mesh, boundary conditions, and displacement calibration (Δy) confirmed that these simplifications have negligible influence on predicted shear rupture and yield capacities. Ductile damage parameters were calibrated from coupon data and verified against experimental stress–strain curves, ensuring reproducibility. Initial geometric imperfections and global buckling were intentionally excluded to focus on local rupture mechanisms; their inclusion, along with residual stress and imperfection sensitivity studies, is recommended for future work.
- Future studies are recommended to include experimental validation
  of welded channel–gusset connections under cyclic loading, to
  examine the influence of geometric imperfections and local buckling,
  and to extend the present findings to other steel grades and
  connection geometries.

#### CRediT authorship contribution statement

**Shervin Maleki:** Writing – review & editing, Supervision, Methodology, Conceptualization. **Kamyab Rezaee:** Writing – original draft, Software, Investigation. **Asal Pournaghshband:** Writing – review & editing, Visualization, Supervision.

#### Declaration of competing interest

The authors declare that they have no known competing financial interests or personal relationships that could have appeared to influence the work reported in this paper.

#### Data availability

No data was used for the research described in the article.

#### References

- C. Clifton, M. Bruneau, G. MacRae, R. Leon, A. Fussell, Steel structures damage from the Christchurch earthquake series of 2010 and 2011, Bull. N Z Soc. Earthq. Eng. 44 (4) (Dec. 2011) 297–318, https://doi.org/10.5459/bnzsee.44.4.297-318.
- [2] G.A. MacRae, G.C. Clifton, M. Bruneau, A. Kanvinde, S. Gardiner, Lessons from Steel Structures in Christchurch Earthquakes, in: Proceedings of the 8th International Conference on Behavior of Steel Structures in Seismic Areas, Shanghai, China, Jul. 2015.
- [3] ANSI/AISC 360-22, Specification For Structural Steel Buildings, American Institute of Steel Construction, Chicago, Illinois, 2022.
- [4] ANSI/AISC 341-22, Seismic Provisions for Structural Steel Buildings, American Institute of Steel Construction, Chicago, Illinois, 2022.
- [5] M. Ghaderi-Garekani, S. Maleki, An investigation of shear failure in welded channel and angle brace members, Structures 45 (Nov. 2022) 1287–1306, https:// doi.org/10.1016/j.istruc.2022.09.103.
- [6] P.J. Fortney, L.S. Muir, W.A. Thornton, Guidance on shear rupture, ductility and element capacity in welded connections, Eng. J. 56 (2) (Jun. 2019) 89–108, https://doi.org/10.62913/engj.v56i2.1146.
- [7] W. Zhang, J. Xie, Y. Liu, Y. Ding, Experimental investigation on steel bracing members with bolted gusset plate connections, J. Build. Eng. 76 (Oct. 2023), https://doi.org/10.1016/j.jobe.2023.107133.
- [8] J. Xie, W. Zhang, Numerical analysis on steel bracing members with bolted gusset plate connections, J. Constr. Steel Res. 222 (Nov. 2024), https://doi.org/10.1016/ j.jcsr.2024.108960.

- [9] J. Shen, O. Seker, M. Faytarouni, B. Akbas, H. Zhang, P. Li, Evaluation of New Seismic provisions for special concentrically braced frames in AISC 341-22, Structures 63 (May 2024), https://doi.org/10.1016/j.istruc.2024.106453.
- [10] A. Rudman, R. Tremblay, C.A. Rogers, Conventional I-shape brace member bolted connections under seismic loading: laboratory study, J. Constr. Steel Res. 184 (Sep. 2021), https://doi.org/10.1016/j.jcsr.2021.106795.
- [11] M. Haddad, N. Shrive, Cyclic performance and fracture of wide flanged concentrically steel braced frames, Aust. J. Struct. Eng. 21 (3) (Jul. 2020) 263–278, https://doi.org/10.1080/13287982.2020.1786988.
- [12] G.A. Riveros, H.N. Mahmoud, S.R. Lopez, Technical Report, The U.S. Army Engineer Research and Development Center (ERDC), Jun. 2019, https://doi.org/ 10.21079/11681/33270.
- [13] N.T. Nguyen, Master of Science in Civil Engineering, Purdue University, 2011.
- [14] C. Topkaya, Block shear failure of gusset plates with welded connections, Eng. Struct. 29 (1) (Jan. 2007) 11–20, https://doi.org/10.1016/j.engstruct 2006 04 003
- [15] S. Maleki, M. Ghaderi-Garekani, Block shear failure in welded gusset plates under combined loading, J. Constr. Steel Res. 170 (Jul. 2020) 106079, https://doi.org/ 10.1016/j.icsr.2020.106079.
- [16] M. Ghaderi-Garekani, S. Maleki, Numerical study of load eccentricity effects on block shear rupture of welded gusset plates, Int. J. Steel Struct. 23 (4) (Aug. 2023) 1148–1163, https://doi.org/10.1007/s13296-023-00758-8.
- [17] M. Ghaderi-Garekani, S. Maleki, Experimental and numerical investigations of block shear failure in gusset plates welded to double angle members, Structures 48 (Feb. 2023) 1356–1372, https://doi.org/10.1016/j.istruc.2023.01.047.
- [18] Y. Song, M. Zhang, K. Ke, M.C.H. Yam, X. Lin, Behavior and design of gusset plates in steel structures: a state-of-the-art review, J. Constr. Steel Res. (211) (2023), https://doi.org/10.1016/j.jcsr.2023.108188.
- [19] W. Zhang, J. Xie, Y. Liu, Y. Ding, Experimental investigation on steel bracing members with bolted gusset plate connections, J. Build. Eng. 76 (2023) 107133, https://doi.org/10.1016/j.jobe.2023.107133.
- [20] Abaqus Software, "Dassault Systemes Simulia Corporation," 2023, France.
- [21] M. Afifi a, R. Tremblay, C.A. Rogers, Numerical & experimental investigation of slotted-hidden-gap connection for square HSS brace members, J. Constr. Steel Res. (192) (2022).
- [22] S. Oosterhof, R.G. Driver, Effects of connection geometry on block shear failure of welded lap plate connections, J. Constr. Steel Res. 67 (2011) 525–532.
- [23] H.T. Zhu, M.C.H. Yam, A.C.C. Lam, V.P. Iu, The shear lag effects on welded steel single angle tension members, J. Constr. Steel Res. 65 (5) (May 2009) 1171–1186, https://doi.org/10.1016/j.jcsr.2008.10.004.
- [24] Y.W. Lee, T. Wierzbicki, Quick Fracture Calibration for Industrial Use, Report No. 115. Impact and Crashworthiness Lab., MIT, 2004.
- [25] ATC24, Guidelines For Cyclic Seismic Testing of Components of Steel Structures, Applied Technology Council, Redwood City, California, USA, 1992.